



Norwegian University of  
Science and Technology

# Antenna measurements of vehicle mounted antennas in the DAB frequency band using an integrated UAV system

**Yngve Tandberg**

Master of Science in Electronics

Submission date: June 2017

Supervisor: Egil Eide, IES

Norwegian University of Science and Technology  
Department of Electronic Systems



# Problem description

Remote controlled drones, also known as multicopters, have recently been used in many new applications and the drones have become increasingly reliable, robust and useful for different purposes. By mounting a small spectrum analyzer on a drone, one can do antenna measurements on larger objects and buildings that otherwise would be difficult to take into an anechoic chamber. Most drones today use precise Global Navigation Satellite System (GNSS) receivers which provide position data that can be collected along with the measured data from the spectrum analyzer.

This thesis explores the ability to use a multicopter with an on-board measurement system to measure the received electric field strength radiated by a stationary transmitting system on different altitudes. Then by using this measurement to develop a radiation pattern for the transmitting antenna.

The task is to design, implement and test a method of measuring the radiation pattern for one or more common types of antennas mounted on a vehicle by using a drone. By introducing the digital audio broadcast (DAB) system in Norway, many car owners mount DAB converters with associated window or roof antennas on their cars. There are few or no descriptions of the radiation pattern of these types of antennas, and there is of great interest to see how such radiation patterns will be in practice. The practical tests will be used to evaluate the feasibility and accuracy of the method by measure and evaluate the radiation patterns.

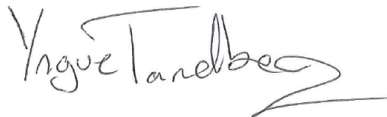
Specifically, the frequency of the measurements is selected to be in the DAB frequency band at (174-240) MHz. Also, the transmitting system uses two types of the common available DAB antennas for vehicles, one roof mounted version with a magnetic base, and one glass mounted on the inside of the windshield. The thesis builds on the previously specialization project [1] from the fall semester of 2016 at the Norwegian University of Science and Technology (NTNU).

---

# Preface

This thesis is the final assignment in my Master of Science programme in Electronics of two years at NTNU. The project was initiated and supervised by Associate Professor Egil Eide from the Department of Electronic Systems at NTNU.

I would like to dedicate this page to thank my supervisor Egil Eide for the helpful guidance through the project, and I would also like to thank the people at the UAV laboratory from the Department of Engineering Cybernetics at NTNU for the helpful assistance of providing the multicopter and equipment for the project.

A handwritten signature in black ink, reading "Yngve Tandberg". The signature is written in a cursive style with a long, sweeping underline.

Yngve Tandberg

Trondheim,  
25. June 2017



# Abstract

In this thesis, it has been designed, constructed and tested an integrated measurement system for performing electric field strength measurements in the far-field, mounted on a drone, known as multicopters. The system uses a small portable spectrum analyzer with a single board computer (SBC) that handles data from the flight controller on the drone and controls the measurements. The method used to solve the project is an experimental approach, a prototype was created to solve the problem. The system is tested and constructed for the Digital Audio Broadcast (DAB) frequency band at 174-240 MHz, using a target frequency of 221.208 MHz. The antennas selected for the measurements were two common DAB antennas for vehicles, one mounted on the roof with a magnetic base and one mounted on the windshield at the driver side.

The measurement results show that there is some inaccuracy due to a low position logging rate of the Global Navigation Satellite System (GNSS) receiver on the drone. The results are used in Matlab to represent the radiation patterns of the antennas in both the azimuth and elevation plane, but with the use of interpolation to define the most likely form of the radiation diagram. It is also possible to see from the results where the directivity of the antennas is pointing.

The results show that the logging of the positions should be improved to create a better resolution of the radiation patterns. It should also be developed a program in Matlab that can display the radiation patterns in three-dimensional graphs, in this way creating a better picture of the coverage of the antennas. Also, to make the system more versatile, it should be tested for other types of antennas and with other frequencies, so it can be explored if the system is durable for all types of antenna measurements.

---



# Sammendrag

I denne masteroppgaven er det blitt designet, utviklet og testet et målesystem for målinger av elektrisk feltstyrke i fjernfeltet som kan brukes på en drone. Det har blitt montert en portabel spektrumanalysator med en minidatamaskin som kan lese informasjon fra dronen og styre utførelsen av målingene. Metoden som ble valgt er en eksperimentell metode, der det ble laget en prototype for å teste teorien bak designet. Målingene er utført i DAB båndet ved 174-240 MHz, med en målerfrekvens på 221.208 MHz. Antennene som ble målt er tilpasset DAB frekvensene og er av to vanlige typer DAB antenner som brukes på biler, en takmontert med magnetfot og en for frontruten montert på innsiden ved førersiden.

Målingene som ble utført viser at det er en viss unøyaktighet grunnet posisjonsloggingens lave innsamlingshastighet på dronen. Resultatene kan forøvrig brukes i Matlab for å representere strålingsdiagrammet for antennene i både asimut- og elevasjonsplanet, men da med bruk av interpolering for å kunne definere den mest sannsynlige formen på strålingsdiagrammet. Det er også mulig å se ut ifra strålingsdiagrammet hvor direktiv antennene er og i hvilke retninger de peker mot.

Resultatene viser at loggingen for posisjonene burde forbedres for å kunne lage strålingsdiagram med bedre oppløsning. Det burde også utvikles et program i Matlab som kan vise strålingsdiagrammene i tredimensjonale grafer for å skape et enda bedre bilde over dekningsområdet til antennene. For å gjøre systemet mer allsidig burde det også testes på flere andre typer antenner og med andre frekvenser slik at det kan utforskes om systemet er holdbart for alle slags typer antennemålinger.



# Definitions

API - Application Programming Interface

CAD - Computer-aided design

DAB - Digital Audio Broadcasting

Drone - Common name for a flying multiple rotors helicopter, in this thesis drones and multicopters are used as the same definition of this type of remote controlled aircraft.

ENU - East (x) North (y) Up (z), local coordinates from Matlab geodetic2enu function

ETSI - The European Telecommunications Standards Institute

FTDI - Future Technology Devices International

GNSS - Global Navigation Satellite System

LGPL - GNU Lesser General Public License

MAVLink - Micro Air Vehicle communication protocol

Multicopter - Helicopter with multiple rotors, often used with a Latin/Greek prefix to represent the number of rotors.

Nkom - Nasjonal kommunikasjonsmyndighet, Norwegian Communication Authority

Omnidirectional radiation pattern - A radiation pattern which radiates in the shape of a toroid with a zero radiation point in the center perpendicular to the maximum directivity direction.

PLF - Polarization loss factor

RBW - Resolution Bandwidth

---

RPAS - Remotely Piloted Aircraft Systems

SBC - Single board computer

UAS - Unmanned Aerial Vehicle Systems

UAV - Unmanned Aerial Vehicle

VBW - Video Bandwidth

VNA - Vector Network Analyzer

VSWR - Voltage standing wave ratio

# Contents

<b>1</b>	<b>Introduction</b>	<b>1</b>
1.1	Background . . . . .	2
1.2	Objectives and goals . . . . .	6
1.3	Equipment . . . . .	7
1.4	Target frequency . . . . .	8
1.5	Structure of the report . . . . .	9
<b>2</b>	<b>Theory</b>	<b>11</b>
2.1	Antenna characterization . . . . .	11
2.1.1	Fundamental parameters . . . . .	11
2.1.2	Friis' transmission equation . . . . .	14
2.1.3	Anechoic chamber . . . . .	15
2.2	Digital Audio Broadcasting . . . . .	16
2.3	Remotely Piloted Aircraft Systems . . . . .	16
2.3.1	Micro Air Vehicle Communication Protocol . . . . .	17
2.4	Graphical visualization of measurements . . . . .	17
2.4.1	Measuring resolution . . . . .	18
<b>3</b>	<b>System design</b>	<b>21</b>
3.1	System architecture . . . . .	21
3.2	Multicopter . . . . .	23
3.2.1	Global Navigation Satellite System receiver . . . . .	24
3.3	Software code . . . . .	24
3.3.1	Workflow . . . . .	24
3.4	Physical design . . . . .	27
3.5	Payload . . . . .	27
3.5.1	Antennas . . . . .	28
3.5.2	CAD model . . . . .	33

## CONTENTS

---

<b>4</b>	<b>Implementation and testing</b>	<b>37</b>
4.1	Antenna tuning . . . . .	37
4.2	Construction . . . . .	40
<b>5</b>	<b>Measurements</b>	<b>43</b>
5.1	Target frequency . . . . .	43
5.2	Drone flight . . . . .	44
5.2.1	Flights . . . . .	46
5.2.2	Magnetic base roof mounted antenna . . . . .	48
5.2.3	Windshield mounted antenna . . . . .	55
<b>6</b>	<b>Data analysis and verification</b>	<b>63</b>
6.1	Method . . . . .	63
6.2	Measurement results . . . . .	64
6.2.1	Resolution and accuracy . . . . .	64
6.2.2	Comparison . . . . .	66
6.3	Error sources and problems . . . . .	67
6.3.1	Interference . . . . .	67
6.3.2	Software problems . . . . .	67
6.4	Improvements and future work . . . . .	68
<b>7</b>	<b>Conclusion</b>	<b>69</b>
	<b>References</b>	<b>70</b>
<b>A</b>	<b>Mission list</b>	<b>75</b>
<b>B</b>	<b>Azimuth plane measurement data at elevation angle <math>\theta = 28^\circ</math></b>	<b>77</b>
B.1	Magnetic base roof mounted antenna . . . . .	78
B.2	Windshield mounted antenna . . . . .	79

# List of Figures

- 1.1 Photos from the LS Telcom report describing the use of a miniature helicopter in antenna measurements [1]. . . . . 3
- 1.2 Illustration of the three modes of operation in the *Drone-Based Field Measurement System* [2]. . . . . 4
- 1.3 Measurement system for the antenna characterization in the report [3] by SixArms. . . . . 5
- 1.4 Antenna characterization of the selected passive antennas from the tests [4], using the frequency range of 195-240 MHz. . . . . 6
- 1.5 The process flow of the thesis project, starting from description to documentation. . . . . 7
- 1.6 Channel 11C as measured in Trondheim. . . . . 9
  
- 2.1 Configuration of antenna measurements inside an anechoic chamber [5]. 16
- 2.2 Package anatomy of the MAVLink protocol [6]. . . . . 17
- 2.3 Concept figure of the flight path for the measurements, where the drone position is given in geographical coordinates North, East and altitude. Then by converting them into a local coordinate system the drone position can be represented by  $(R, \phi, \theta)$ , where  $\phi$  is the azimuth angle and  $\theta$  is the elevation angle. . . . . 18
- 2.4 Cross section of the first quadrant of the elevation plane, showing two points from the waypoint circles and the angle ( $\theta$ ) between them. . . . . 19
  
- 3.1 Total system overview with the UAV subsystem on the left, and the measurement subsystem communicating with the drone on the right side. 22
- 3.2 DJI S1000+ octocopter with size measurements from the user manual [7]. 23
- 3.3 Process block diagram of the program code. . . . . 25
- 3.4 DAB magnetic base antenna for vehicles [8]. . . . . 28
- 3.5 DAB windshield mounted active antenna [9] illustrated mounting on the test vehicle Opel Astra G estate [10]. . . . . 29
- 3.6 Dimensions and radiation pattern for the HE2M helical whip antenna [11]. 31
- 3.7 Reference length measurement for the cutting length. . . . . 32

## LIST OF FIGURES

---

3.8	Bottom view of the proposed measurement subsystem with dimensions given in mm of the sides. . . . .	34
3.9	Side view of the measurement subsystem with all main components assembled in the correct order, without cables and connectors. . . . .	35
3.10	An exploded view of the measurement subsystem pointing downwards. . . . .	35
3.11	A complete illustration of the measurement subsystem assembled onto the mounting bracket of the DJI S1000 [12][13]. . . . .	36
4.1	The response of S11 over the frequency range (100-300) MHz of the flexible helical whip antenna before tuning, marking the resonance frequency at 152.853 MHz. . . . .	38
4.2	Final length of the helical whip antenna. . . . .	39
4.3	Before and after picture of the tuning process. . . . .	39
4.4	The response of S11 over the frequency range (100-300) MHz of the flexible helical whip antenna after tuning, marking the resonance frequency at 221.208 MHz. . . . .	40
4.5	Perspective upside view of the assembly, the antenna is positioned as the back side of the system. . . . .	41
4.6	Side view of the complete assembly. . . . .	42
4.7	A top view of the system connected to the test flight controller to the right. . . . .	42
5.1	A frequency sweep showing the DAB frequency channel 11C for Sør-Trøndelag with the selected frequency for the measurements positioned outside of the channel band. . . . .	43
5.2	A detailed view of the upper part of channel 11C with the selected measurement frequency positioned outside of the band. . . . .	44
5.3	Angular placement of the vehicle 60° from the North axis, with dots marking antenna positions, blue windshield mounted and red magnetic base mounted. Home position is set at the center of the vehicle. . . . .	45
5.4	Picture of the vehicle and location used for the measurements. . . . .	45
5.5	Picture of the multicopter when measuring the magnetic base roof antenna. . . . .	46
5.6	GNSS position log data of the flight path when measuring the magnetic base roof mounted antenna, antenna position in red dot and rings at elevations $\theta = [7^\circ, 16^\circ, 28^\circ, 46^\circ, 59^\circ, 67^\circ, 77^\circ, 87^\circ]$ . . . . .	47
5.7	GNSS position log data of the second flight path when measuring the windshield mounted antenna, antenna position in blue dot and rings at elevations $\theta = [8^\circ, 28^\circ, 44^\circ, 58^\circ, 67^\circ, 76^\circ, 87^\circ]$ . . . . .	48
5.8	Placement of the magnetic base antenna close to existing antenna on the vehicle, which is disassembled under the measurements. The home position is also shown to be at the middle of the vehicle roof. . . . .	49



5.9	GNSS positions of the flight for the magnetic base antenna at elevation angle $\theta = 28^\circ$ , with the circles marking the sampled position and the antenna position marked as the red dot. Markers shows two subsequent samples used to calculate the angle between them. . . . .	50
5.10	A polar diagram of the normalized radiation pattern for the magnetic base antenna, plotted in the azimuth plane at elevation $\theta = 28^\circ$ , with the red line indicating the angular position of the vehicle pointing at $60^\circ$ . . .	51
5.11	Normalized radiation pattern of the magnetic base antenna shown in the elevation plane at azimuth angles ( $\phi = 355^\circ, 175^\circ$ ). . . . .	52
5.12	Normalized radiation pattern of the magnetic base antenna shown in the elevation plane at azimuth angles ( $\phi = 50^\circ, 225^\circ$ ). . . . .	53
5.13	Normalized radiation pattern of the magnetic base antenna shown in the elevation plane at azimuth angles ( $\phi = 85^\circ, 270^\circ$ ). . . . .	54
5.14	Normalized radiation pattern of the magnetic base antenna shown in the elevation plane at azimuth angles ( $\phi = 145^\circ, 320^\circ$ ). . . . .	55
5.15	Placement of the windshield antenna on at the left side of the vehicle windshield grounded to the chassis at the window pillar and positioned from 20 cm to 35 cm down from the roof with an angle of about $60^\circ$ from the altitude axis. . . . .	56
5.16	GNSS ENU positions of the drone flight path for the windshield antenna at elevation angle $\theta = 28^\circ$ , with the circles marking the sampled position and the antenna position marked as the red dot. Markers shows two subsequent samples used to calculate the angle between them. . . . .	57
5.17	The normalized radiation pattern for the windshield antenna, plotted in the azimuth plane at elevation $\theta = 28^\circ$ , with the red line indicating the angular position of the vehicle pointing at $60^\circ$ . . . . .	58
5.18	Normalized radiation pattern of the windshield antenna shown in the elevation plane at azimuth angles ( $\phi = 355^\circ, 175^\circ$ ). . . . .	59
5.19	Normalized radiation pattern of the windshield antenna shown in the elevation plane at azimuth angles ( $\phi = 50^\circ, 225^\circ$ ). . . . .	60
5.20	Normalized radiation pattern of the windshield antenna shown in the elevation plane at azimuth angles ( $\phi = 85^\circ, 270^\circ$ ). . . . .	61
5.21	Normalized radiation pattern of the windshield antenna shown in the elevation plane at azimuth angles ( $\phi = 145^\circ, 320^\circ$ ). . . . .	62

## LIST OF FIGURES

---

# List of Tables

2.1	Table showing the requirements for the RPC4 configuration in DAB systems [14][15]. . . . .	16
3.1	Key specifications of the DJI S1000+ octocopter taken from the user manual [7]. . . . .	24
3.2	Timing test of some selected number of samples executed by the program.	26
3.3	Specifications of DAB magnetic base antenna for vehicles. [8] . . . . .	29
3.4	Specifications of DAB windshield mounted antenna for vehicles [9]. . .	30
3.5	Specifications of HE2M helical whip antenna [11]. . . . .	32
3.6	Cutting table for the HE2M helical whip antenna. . . . .	32
3.7	Compensation dB table from the angular dB reduction of the radiation pattern of the flexible helical whip antenna. . . . .	33
5.1	Calculated radius and altitudes used for the mission list for the drone under flight. . . . .	46
A.1	Waypoint list for the GNSS positions used for the measurements. . . . .	75
B.1	Measurements results for the magnetic base roof mounted antenna in the azimuth plane at elevation angle $\theta = 28^\circ$ . . . . .	78
B.2	Measurements results for the windshield mounted antenna in the azimuth plane at elevation angle $\theta = 28^\circ$ . . . . .	79

## LIST OF TABLES

---

# Chapter 1

## Introduction

Today, the common way to characterize an antenna is to measure and calculate some of the fundamental parameters, such as the resonance frequency, scattering parameters ( $S_{i,j}$ ), impedance ( $Z$ ), voltage standing wave ratio (VSWR), the radiation pattern, radiation efficiency ( $\epsilon_R$ ), gain (G) and the directivity (D). To measure these parameters typically a vector network analyzer (VNA) is used, and to characterize the radiation pattern it usually have to be performed inside an anechoic chamber, which is a special designed room for blocking out interference, and absorbing reflections with absorbing elements placed on the surfaces of the room. A more detailed explanation of how an anechoic chamber works is described later on in chapter 2.

By using an anechoic chamber one is restricted by the range of frequency, usually at the lower frequencies that can be absorbed into the absorbing elements due to physical size restrictions. These rooms can cost a significant amount of money to build and maintain, and the measurements done inside of them will only show the radiation pattern of the antenna when it is not affected by any surrounding objects. Therefore it will be of interest to see if the use of a drone or an unmanned aerial vehicle system (UAV,UAS) to measure the antenna on the site of installation will be as good or worse than when the measurement is performed inside an anechoic chamber.

In this chapter some background about drones and some existing research based on the use of drones in antenna measurements is presented, then the objectives and goals for the project is explained before the structure of the thesis is described.

## 1.1 Background

Over the last few years remotely piloted aircraft systems, have become a popular utility tool to both professionals and the common hobbyist. This popularity may be because of the reduced price for a sophisticated remote controlled multicopter, but also due to the development of the action camera that lets the user mount their camera on different objects and record their action videos in high definition quality. This combination of integrating an action camera into a multicopter is a relative new trend for most hobbyists, but the solution has existed for many years and mainly used in military applications as in aerial reconnaissance e.g. the MQ-1 Predator [16] build by General Atomics [17] and used by the United States Air Force [18]. Since the technology is now at a more affordable level for most people the trend seems to be boosting the development of better and more advanced multicopters as seen with the company DJI [19]. At the professional side of this new development the use of unmanned aerial vehicle systems have also grown to be popular mostly with the use of camera for television coverage in sports events, but also other on-board equipment with sensors and measurement tools used for inspection, measurement and other similar operations.

The usage of drones in antenna measurements is not so common yet, but some previously research have been performed with this purpose. In 2012 an experiment [20] was conducted by a group at the university Politecnico di Torino together with the research organization Consiglio Nazionale delle Ricerche. They used a multicopter to measure the antenna radiation pattern together with a topographic tracking device with a motorized total station, which is a modern surveying instrument in order to define the absolute position of the drone. The drone used for the measurements was a hexacopter<sup>1</sup> with some customized construction for the antenna and positioning system placed underneath the body of the drone. The results were promising but not conclusive and some more research had to be done.

Another research [1] from 2012 performed by LS Telcom used a miniature helicopter in an unmanned aerial system (UAS) with an on board radio frequency spectrum analyzer, and measured the received electric field strength on different altitudes to characterize the radiation pattern of the target antenna. The system was developed over a five years period and developed into a sophisticated system with about a hundred parameters that had to be coordinated during flight. The images shown in figures 1.1a and b is from the report shows the miniature helicopter used and the flight path from the measurements.

---

<sup>1</sup>Six-rotors multicopter.



(a) Miniature helicopter used in the research with measurement system mounted under the landing skids.



(b) Flight path of the measurements around the antenna illustrated with a geographical representation.

Figure 1.1: Photos from the LS Telcom report describing the use of a miniature helicopter in antenna measurements [1].

The concept of antenna measurements with the use of multicopters has also been discussed in later years. In an online website post [2] by Kirt Blattenberger, he discusses and describes a system that uses a multicopter for measuring light intensity, sound levels and radio frequencies in three different modes of measurement. One mode is where the drone is measuring on given Cartesian coordinates to create a three-dimensional map, another mode is by setting the drone to measure equipotential surfaces to create a surface map. The illustration he presents is shown in figure 1.2.

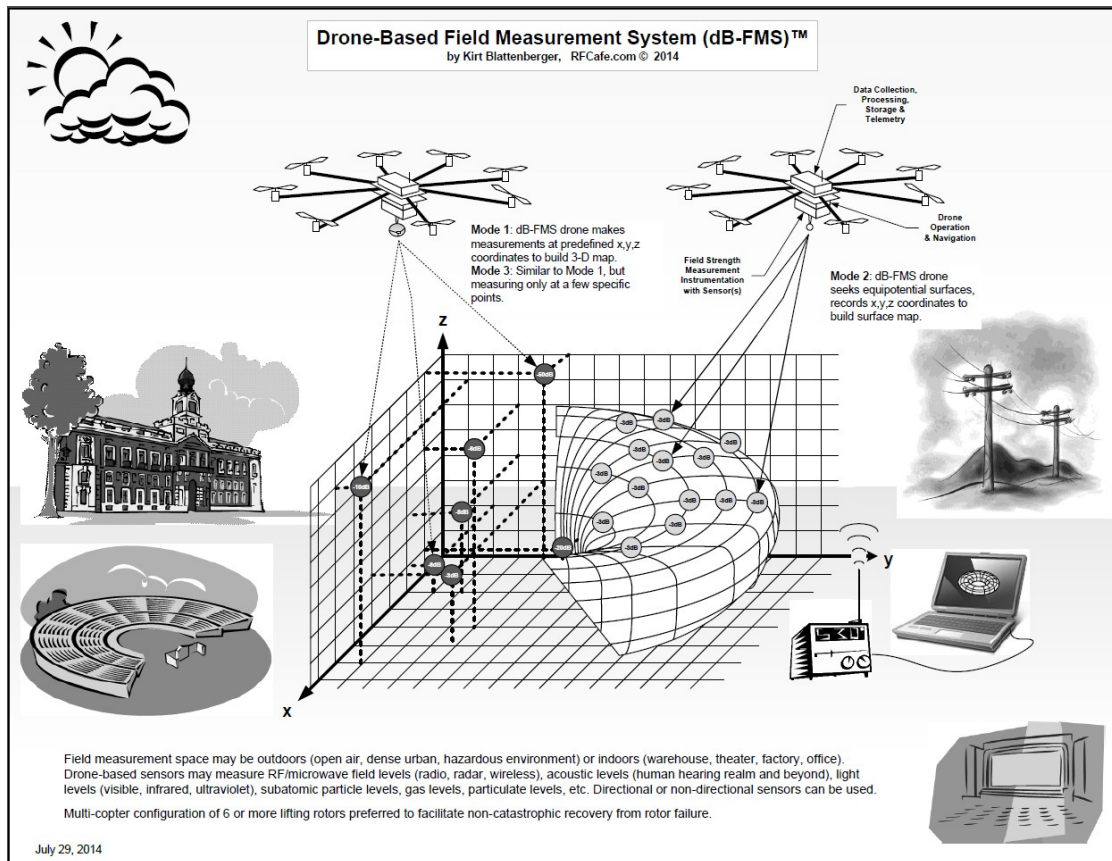


Figure 1.2: Illustration of the three modes of operation in the *Drone-Based Field Measurement System* [2].

There is also some companies that provides this type of measurement service, as the Australian company SixArms, previously known as Innovative Drone Solutions from the specialization report [5], they published a report [3] late 2015, where they present a measurement system with a spectrum analyzer integrated on a drone with the measurement antenna on top of the aircraft. The figure 1.3 shows how the system was set up from the report.



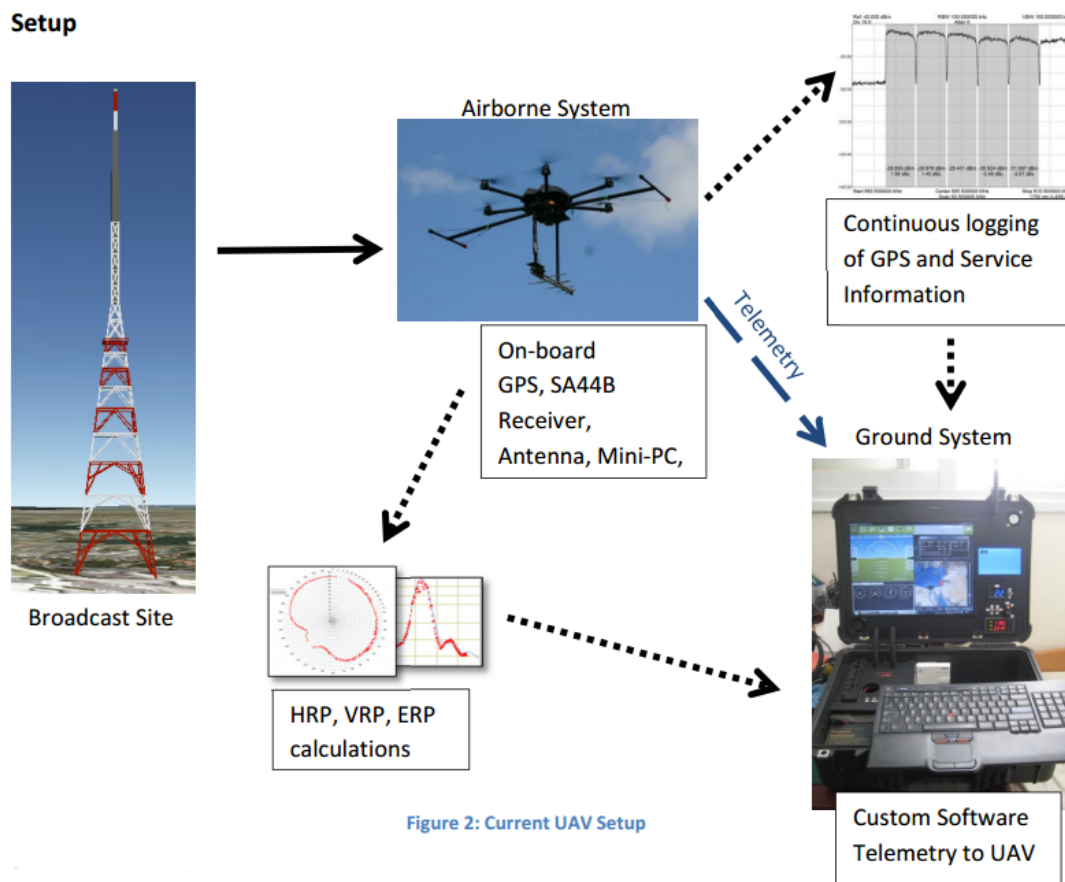


Figure 1.3: Measurement system for the antenna characterization in the report [3] by SixArms.

Since this thesis will be based around antenna measuring with drones and by measuring at a frequency selected in the DAB frequency band, it will also be interesting to look at the research [4] by the Norwegian Communications Authority [21] (Nkom) in 2016. The Norwegian government decided [22] to shut down the FM radio broadcast network and convert to the DAB+<sup>2</sup> radio broadcast system by 2017, but some issues during the conversion concerning the reception quality and coverage of the radio signals have been reported to be poor for vehicles, often because of the selected antenna and adapter solution. Because of this problems a request was issued to Nkom to measure, test and document the reception and quality of the DAB radio signals with the use of some commonly sold DAB+ radio adapters and antenna solutions. The report is based on

<sup>2</sup>DAB+ uses the same frequency band as DAB, but uses the MPEG-4 High Efficiency Advanced Audio Coding v2 (HE-AACv2) [23].

measuring the received power on different frequencies in the DAB+ band and some of the results from the tests of the passive antennas is shown in figure 1.4.

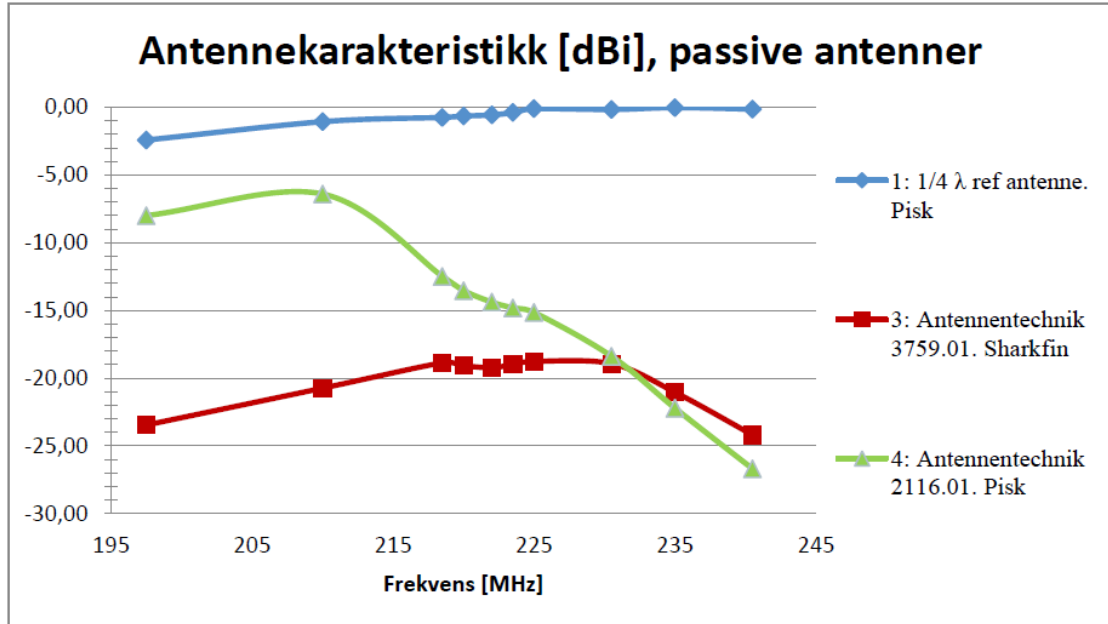


Figure 1.4: Antenna characterization of the selected passive antennas from the tests [4], using the frequency range of 195-240 MHz.

All of this research shows that antenna measurements of the future have the potential to be resolved by using drones and the more wireless systems that are installed, the more will the need to control and map the radiation coming from the installations in order to avoid interference and optimizing performance of the systems.

## 1.2 Objectives and goals

The main objective for this thesis is to utilize and use a multicopter for measurements and characterization of a transmitting antenna mounted on a vehicle. The measurements will be performed by measuring the received power radiated from the transmitting antenna, which is positioned in the far field in relation to the flight path of the multicopter. The transmitting antenna mounted on the vehicle is tuned for the DAB frequency band (174-240 MHz) and the measuring system will have to be tuned to this frequency band. The results will be plotted and evaluated as radiation patterns in the azimuth plane and the elevation plane to see how the accuracy of the measurements is in the radiation patterns.

The goals for the project are as following:

1. Design a measurement system using a portable spectrum analyzer and integrate it onto an existing multicopter system.
2. Code a program that can read the telemetry data broadcasted from the flight controller to store the flight position log, and control the on-board computer to perform the measurements with a portable spectrum analyzer.
3. Construct the necessary hardware to be able of mounting the equipment on the multicopter.
4. Measure the received power from a vertical linear polarized antenna in the far field and in the electric field from a transmitting system on a vehicle.
5. The measurements are to be performed in a hemispherical form so the data can be represented into one azimuth plane radiation pattern and in four elevation plane radiation patterns of the measured sphere for each antenna.
6. Process and discuss the measured data in terms of the accuracy and readability of the radiation patterns.

A simple process flow of the thesis is presented in the figure 1.5 below, this shows how the whole process is executed starting by the project description, then the project design will see if the description needs to be adjusted before proceeding to the measurements. After measurements the data is analyzed, then if more data needs to be evaluated it will be reprocessed before the documentation of the project.

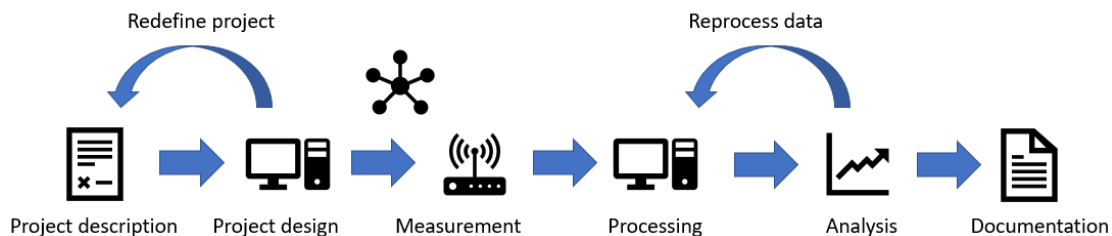


Figure 1.5: The process flow of the thesis project, starting from description to documentation.

### 1.3 Equipment

Since this thesis builds upon the research from the previously specialization project [5], some of the equipment will be used again to minimize the cost of the project. The equipment already provided is as following.

- DJI S1000+ multicopter [12], provided by the UAV laboratory at the Department of Engineering Cybernetics at NTNU.
- Pixhawk PX4 flight controller [24], used on the multicopter.
- 3DR u-blox GNSS receiver [25] for logging the flight path positions on the multicopter.
- USB-SA44B 1 Hz to 4.4 GHz spectrum analyzer from Signal Hound [26], used with the multicopter on the measurement subsystem.
- USB-TG124 100 kHz to 12.4 GHz tracking generator capable of generating a narrow banded signal with amplitudes from -30 dBm to -12 dBm, from Signal Hound [26], used with the transmitting antenna on the vehicle.
- Odroid XU4, is a single-board computer (SBC) from Hardkernel [27], used for controlling and handling communication with the flight controller and spectrum analyzer.
- Test vehicle, Opel Astra G estate provided by the author.

### **1.4 Target frequency**

For the DAB radio conversion in Norway the channels in the DAB frequency band is divided and given out into regions of the land as the report from Nkom shows [28]. The target frequency in this thesis is selected to be close to the DAB channel 11C allocated in Sør-Trøndelag, which is in the range 219,584-221,120 MHz. A survey of the frequencies in Trondheim figure 1.6 shows the channel 11C.

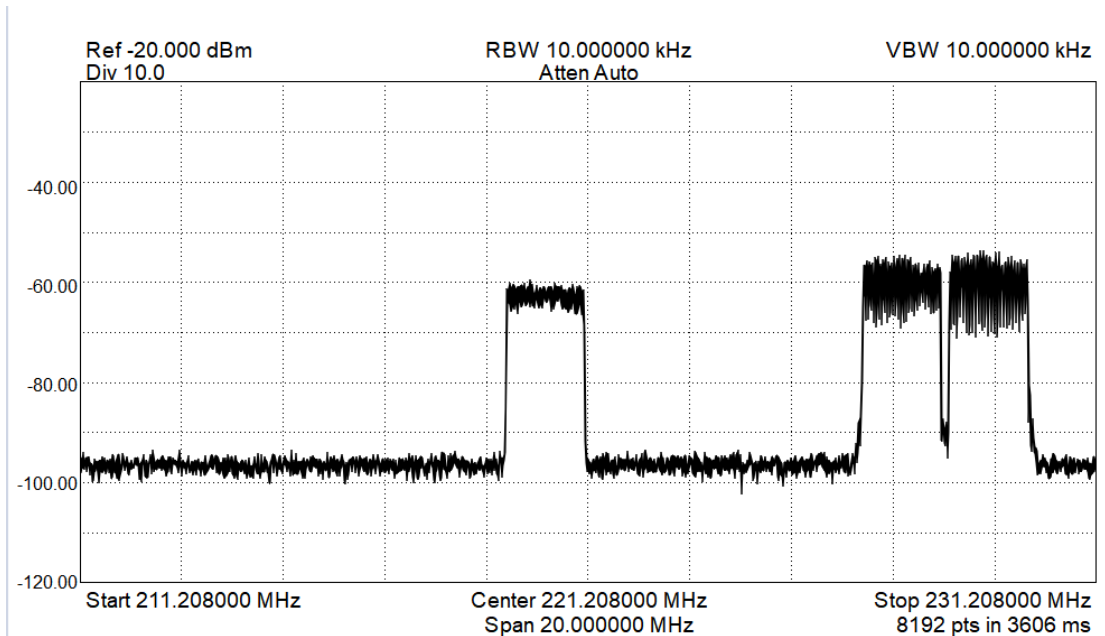


Figure 1.6: Channel 11C as measured in Trondheim.

The neighbouring channel above channel 11C is 11D from 221,296-222,832 MHz is not present at the figure 1.6 which is the area west of Trondheim called Fosen. The target frequency is set to be 221.208 MHz which is just outside channel 11C and under channel 11D.

## 1.5 Structure of the report

To give an overview of the structure of this thesis a brief explanation of each following chapters is presented here.

- Chapter 2 Theory, covers some useful background theory about how antenna measurements is commonly done, then a section explaining the digital audio broadcast system, before some information of the multicopter communication system is presented and at last it is presented some formulas used for the measurements.
- Chapter 3 System design, presents the architecture for the system before the program code block diagram. Then the design of the implementation is described based of the wanted specifications from the problem description. Some information of the antennas is presented before the last section presenting the physical design is proposed for the implementation.

- Chapter 4 Implementation, starts with the tuning of the helical whip antenna before the implementation of the design from chapter 3 is presented and how it was realized.
- Chapter 5 Results, presents measurements of the target frequency and proves that it is not interfering with the DAB radio broadcast, then the drone flight is presented starting with the positioning of the target vehicle. First the measurements of the magnetic base roof mounted antenna is presented, then the windshield mounted antenna.
- Chapter 6 Discussion, starts with a discussion of the method used for the project, before discussing the results from the measurements in terms of accuracy and faults. Then a comparison of the antennas are made before discussing some error sources and problems in the project. For a last section the improvements and future work is proposed for the project.
- Chapter 7 Conclusion, the last chapter concludes the project by looking back at the problem description of the project and gives an overall conclusion of the solution presented in this thesis.

# Chapter 2

## Theory

In this chapter some theory for the thesis is explained in detail as a supplement in order to use it later for the discussion of the measurement results. As a start the characterization of antennas is explained with the fundamental parameters before Friis' transmission equation is presented. It is also described a section about the DAB technology since the frequency selected for this project is in its frequency band and will be also used in the discussion part in terms of signal coverage. Then a section explaining the drone system, the protocol for controlling and configuring the drone. As a last section, some formulations to calculate the resolution and accuracy of the measurements is explained.

### 2.1 Antenna characterization

As mentioned in the introduction when characterizing an antenna it is desirable to know some of the fundamental parameters of the antenna. This can usually be achieved through testing and measuring using a vector network analyzer and using an anechoic chamber for the radiation pattern.

#### 2.1.1 Fundamental parameters

The parameters described here is taken from the online resource [29], the text book [30] and the text book [31] and they are presented in the order of how they are connected starting with the input impedance. All parameters are frequency dependent and the choice of frequency is usually the resonance frequency of the antenna.

- Input impedance, is the impedance between the input terminals of the antenna or the ratio between voltage and current at the terminals, or it can also be the ratio between appropriate components of the electric and magnetic field at a point. [31] [32]. The impedance ( $Z_A$ ) consists of a real part ( $R_A$ ) and an imaginary part ( $jX_A$ ), where A indicating it is the antenna impedance and ( $X_A$ ) is

the reactance of either a capacitance (negative X) or an inductance (positive X). The impedance is also frequency dependent and usually described with a angular frequency  $\omega = 2\pi f$ .

$$Z_A(\omega) = R_A \pm jX_A(\omega) [\Omega] \quad (2.1)$$

- Resonance frequency, is the frequency where the imaginary part of the impedance is zero and the impedance is pure ohmic. This frequency is also where the antenna will radiate at maximum [30].
- Reflection coefficient ( $\Gamma$ ), the coefficient which describes the ratio between the normalized amplitude of the reflected voltage wave ( $V_0^-$ ) to the amplitude of the incident voltage wave ( $V_0^+$ ) [30] see equation 2.2, it can also be derived into the relation between the added impedance ( $Z$ ), from either a load impedance ( $Z_L$ ) or a source impedance ( $Z_S$ ) and the standard system reference impedance ( $Z_0$ ) with a value of 50  $\Omega$ .

$$\Gamma = \frac{V_0^-}{V_0^+} = \frac{Z - Z_0}{Z + Z_0} \quad (2.2)$$

- Scattering parameters ( $S_{i,j}$ ), like the impedance describes the relation between two port terminals, but unlike impedance which uses the ratio between voltage and current the s-parameters relates to the voltage waves of the incident ( $V_j^+$ ) and the reflected ( $V_i^-$ ) to characterize the system [30]. The s-parameters are useful for higher frequencies because it is harder to measure voltage and currents at these frequencies and easier to measure the incident ( $V_j^+$ ) and reflected ( $V_i^-$ ) wave. The s-parameters are usually shown in a matrix and shows the different relationships of the system, see equation 2.3 below for a overview of a NxN s-parameter matrix as shown in the text book [30].

$$\begin{bmatrix} V_1^- \\ V_2^- \\ \cdot \\ \cdot \\ \cdot \\ V_N^- \end{bmatrix} = \begin{bmatrix} S_{1,1} & S_{1,2} & \cdot & \cdot & \cdot & S_{1,N} \\ S_{2,1} & \cdot & \cdot & \cdot & \cdot & \cdot \\ \cdot & \cdot & \cdot & \cdot & \cdot & \cdot \\ \cdot & \cdot & \cdot & \cdot & \cdot & \cdot \\ \cdot & \cdot & \cdot & \cdot & \cdot & \cdot \\ S_{N,1} & \cdot & \cdot & \cdot & \cdot & S_{N,N} \end{bmatrix} \cdot \begin{bmatrix} V_1^+ \\ V_2^+ \\ \cdot \\ \cdot \\ \cdot \\ V_N^+ \end{bmatrix} \quad (2.3)$$

For a selected element of the matrix equation 2.4 can be used [30].

$$S_{i,j} = \left. \frac{V_i^-}{V_j^+} \right|_{V_k^+ = 0 \text{ for } k \neq j} \quad (2.4)$$

- Voltage standing wave ratio (VSWR), uses the relationship of the reflection coefficient to show how much of the incoming voltage wave will be reflected or



absorbed into the impedance of the antenna [29].

$$VSWR = \frac{1 + |\Gamma|}{1 - |\Gamma|} \quad (2.5)$$

- Antenna efficiency ( $\epsilon_0$ ), is a measure of the overall efficiency of the antenna and consists of three types of efficiencies.

$$\epsilon_0 = \epsilon_r \epsilon_c \epsilon_d \quad (2.6)$$

The reflection efficiency ( $\epsilon_r$ ), tells the how the efficiency of the reflection coefficient ( $\Gamma$ ) between the transmission line and the antenna [31] is matched as equation 2.7 shows.

$$\epsilon_r = 1 - |\Gamma|^2 \quad (2.7)$$

The other two is the conductivity efficiency ( $\epsilon_c$ ) and the dielectric efficiency ( $\epsilon_d$ ), which is two factors that can be determined by experimenting and is not separable. The two factors are usually expressed as the antenna efficiency ( $\epsilon_{cd}$ ). The total radiated power ( $P_{rad}$ ) according to [31] can be expressed as the product between the total input power ( $P_{in}$ ) and the antenna efficiency ( $\epsilon_{cd}$ ) as shown in equation 2.8.

$$P_{rad} = \epsilon_{cd} P_{in} \quad (2.8)$$

- Radiation pattern, is the radiation diagram of the antenna and shows how and in what directions the antenna radiates or receives the field strength, usually in decibels either in the electric E-field or in the magnetic H-field. For two dimensional patterns it is necessary to explain what plane the diagram is plotted in, either the azimuth plane ( $\phi$ ) or in the elevation plane ( $\theta$ ). The radiation pattern also describes the antenna at only the selected frequency, and in order to cover multiple frequencies it is necessary to perform several measurements on each selected frequency.
- Directivity (D), previously called directive gain is described as *"the ratio of the radiation intensity in a given direction from the antenna to the radiation intensity averaged over all directions."* [31][32] It is usually compared with how much of the maximum peak of radiation ( $U_{max}$ ) is in relation with an isotropic radiation pattern ( $U_0$ ). Equation 2.9 shows the directivity (D) is equal to the maximum radiation intensity ( $U_{max}$ ) divided on the total radiated power ( $P_{rad}$ ) over  $4\pi$ .

$$D = \frac{U}{U_0} = \frac{4\pi U_{max}}{P_{rad}} \quad (2.9)$$

- Gain (G), the gain is related to the directivity (D) and uses the antenna efficiency ( $\epsilon_{cd}$ ) in the conversion between them. Gain is a measure of how much the antenna radiates in the given direction in relation to an reference antenna, usually an isotropic antenna and uses the unit dBi, but is often just used as dB. It can also use in relation to a dipole antenna and will then be denoted as dBd which corresponds to 2.15dBi [31].

$$G = \epsilon_{cd} D \quad (2.10)$$

- Polarization, of an antenna is defined as the orientation of the radiation wave when emitted from the antenna. [31] For this thesis only linear polarization is presented, and is cited as *A time-harmonic wave is linearly polarized, at a given point in space, if the electric-field (or magnetic-field) vector at that given point is always oriented along the same straight line at every instant of time* [31, p. 70]. The polarization can be written as equation 2.11 shows, where the incoming wave ( $E_i$ ) in the electric field ( $\bar{E}_i$ ) is multiplied with the polarization unit vector ( $\hat{\rho}_w$ ).

$$\bar{E}_i = \hat{\rho}_w \cdot E_i \quad (2.11)$$

- Polarization loss factor (PLF), is used when two antennas transmitting and receiving to each other and if they are not positioned in alignment with each other there will be a polarization mismatch and a loss. [31] The loss factor can be calculated by using the polarization (p) angle ( $\psi_p$ ) between the antennas,  $\hat{\rho}_w$  is the unit vector of the wave and  $\hat{\rho}_a$  is the unit vector of the antenna. The following equation 2.12 shows the PLF. [31][29]

$$PLF = |\hat{\rho}_w \cdot \hat{\rho}_a|^2 = |\cos(\psi_p)|^2 \quad (2.12)$$

### 2.1.2 Friis' transmission equation

Friis' transmission equation is one of the most iconic equations used when calculating a transmission link budget. The equation is used to tell how much power can be received based on how much power is transmitted between two antennas over a distance (R) in the far-field, where the distance (R) needs to be larger than the double of the square of the dimension (D) of the antenna over the wavelength ( $\lambda$ ) as equation 2.13 shows.

$$R > \frac{2D^2}{\lambda} \quad (2.13)$$

The equation is also related to the free-space path loss (FSPL) which is the loss of the signal strength due to the wave traveling through free space and is shown in equation 2.14.

$$FSPL = \left(\frac{\lambda}{4\pi R}\right)^2 \quad (2.14)$$

Using the derived expression from [31] of the whole Friis' transmission equation, as the following equation 2.15 shows. The received power ( $P_r$ ) is equal to the transmitted power ( $P_t$ ) times transmitter antenna gain ( $G_t$ ), receiving antenna gain ( $G_r$ ), the free-space path loss (FSPL) and last multiplied by the polarization loss factor (PLF).

$$P_r = P_t G_t G_r \left(\frac{\lambda}{4\pi R}\right)^2 |\cos(\psi_p)|^2 \quad (2.15)$$

The equation could also include the impedance mismatch of the system, but is not included here as it would not be relevant for the calculations and verification later. Equation 2.15 can also be presented in logarithmic notation as following equation 2.16 shows.

$$P_r = P_t + G_t + G_r + 20 \log\left(\frac{\lambda}{4\pi R}\right) + 20 \log(|\cos(\psi_p)|) \quad (2.16)$$

Where  $P_r$  and  $P_t$  is given in (dBm),  $G_r$ ,  $G_t$ , FSPL and PLF is given in (dB).

### 2.1.3 Anechoic chamber

In an ideal antenna measuring environment there is no interference coming from reflections or other sources around the measuring site, and the noise floor level is so low that it does not impact the measurements. To create this type of environment will require a huge empty space which is not realizable, therefore it has been developed an anechoic room [33] for to represent somewhat this kind of environment. The anechoic room or chamber is a room with radio frequency shielding on or inside the walls to block out interfering sources from outside the room. Since the room will keep out the interfering sources means that it will keep the radiating source inside the room from escaping and thus cause interference due to reflections. To overcome this problem the surfaces of the room gets covered with radio frequency absorbing elements which works as a receiving antenna with a shortened load in the end of an quarter wave transmission line. An example of an anechoic chamber is shown in figure 2.1.

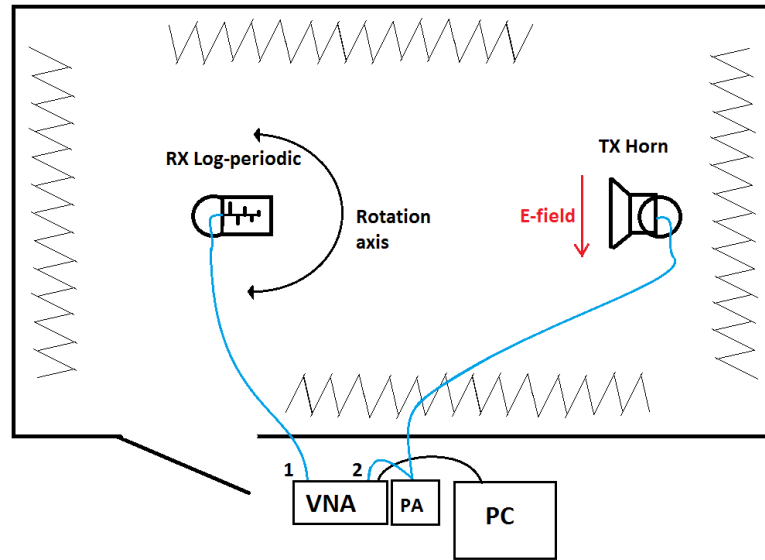


Figure 2.1: Configuration of antenna measurements inside an anechoic chamber [5].

## 2.2 Digital Audio Broadcasting

The DAB system in Norway uses the frequency band 174-240 MHz and is regulated by two international agreements [14]. The frequencies in the lower part 174-230 MHz is regulated by the GE06 agreement [15], and according to the configuration RPC4 [14] which sets the requirements for coverage of mobile receivers outdoors as vehicles with antenna mounted on the roof, see table 2.1 for specifications of this standard.

Signal to noise ratio, S/N	15 dB
Minimum field strength ( $E_{med})_{ref}$ at 10 m altitude	60 dB ( $\mu V/m$ )
Minimum field strength at 1.5 m altitude	48 dB ( $\mu V/m$ )

Table 2.1: Table showing the requirements for the RPC4 configuration in DAB systems [14][15].

## 2.3 Remotely Piloted Aircraft Systems

The multicopter used for the project can be controlled by an operator and it can control it self autonomously due to the advanced flight controller, which acts much like a single board computer. When talking about UAV or UAS, it is also characterized as an remotely piloted aircraft system (RPAS) since an operator can and usually have to control the aircraft in some way.

The communication in these type of systems is commonly used through a ground station which transmits commands and receives status from the flight controller. One type of protocol used for this communication is the Micro Air Vehicle Communication protocol (MAVLink) [6] and in this project the MAVLink protocol is used.

### 2.3.1 Micro Air Vehicle Communication Protocol

The micro air vehicle communication protocol [6] is a protocol developed and released by Lorenz Meier in 2009 under the Lesser General Public License (LGPL). The protocol is based on sending header only packages of commands through a serial link that holds multiple variables of information and action requests. The protocol was constructed to use with a ground control computer that communicates with the UAV autonomously. Figure 2.2 shows the packages of the protocol.

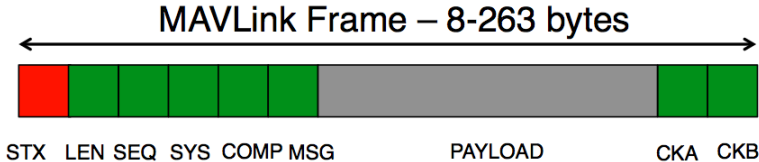


Figure 2.2: Package anatomy of the MAVLink protocol [6].

For this project the MAVLink protocol is implemented into the main code as a header reference, and uses some standard serial read functions in C to read the packages and control that it is MAVLink with the parsing command implemented in the header.

## 2.4 Graphical visualization of measurements

When the drone is flying it will read and log the GNSS data. This data is given in geographical coordinates as latitudes and longitudes in degrees. By using Matlab, the coordinates can be converted into local Cartesian coordinates or in spherical coordinates. Since the measurements are to be performed by flying in a hemispherical form, the easiest way is to divide the hemisphere into horizontal disks and fly in circles with a changing altitude to represent the hemisphere. A concept figure describing the measurement flight path is shown in figure 2.3. The coordinates given by the GNSS receiver is in geographical coordinates in degrees North, East and altitude. These coordinates can be converted into a local coordinate system for the measurement site and the drone position can be given with the radius ( $R$ ), azimuth angle ( $\phi$ ) and elevation angle ( $\theta$ ) from the origin of where the transmitting antenna is positioned. The sliced disks of the hemisphere are shown as the black dashed lines.

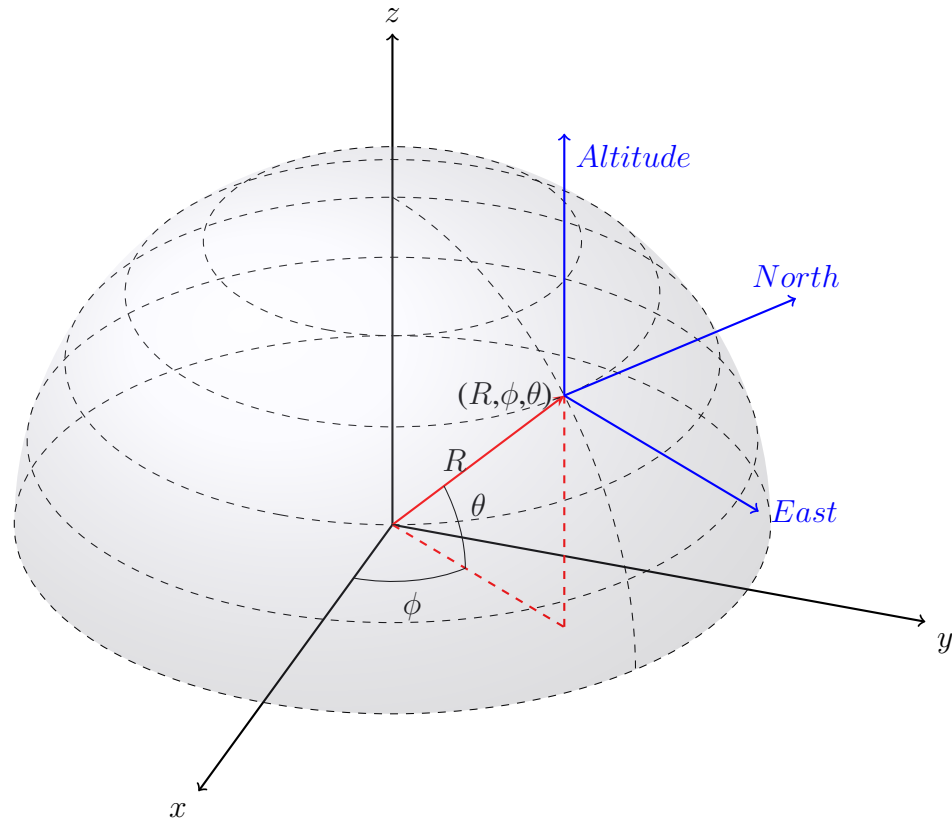


Figure 2.3: Concept figure of the flight path for the measurements, where the drone position is given in geographical coordinates North, East and altitude. Then by converting them into a local coordinate system the drone position can be represented by  $(R, \phi, \theta)$ , where  $\phi$  is the azimuth angle and  $\theta$  is the elevation angle.

Using the concept figure 2.3 the drone starts at the bottom dashed ring, measures while flying a whole circle, then moves upwards along  $z$  axis to the next circle and repeats until it reaches the top and finishes. This method makes it easy to plot the radiation pattern in the azimuth plane ( $\phi$ ) for each circle, and to make a cross section in the elevation plane ( $\theta$ ), two angles with  $180^\circ$  between each other in the azimuth plane ( $\phi$ ) is selected as start and stop points, then all points in the elevation ( $\theta$ ) can be sampled and displayed as the radiation pattern in the elevation plane ( $\theta$ ).

### 2.4.1 Measuring resolution

When using the previously mentioned method from figure 2.3 to acquire the measurements, the multicopter needs to have a radius and altitude for each circle implemented into a waypoint list before flight. To be able to get these functions, one can use the fig-

Figure 2.4 with a cross section of the first quadrant of the elevation plane from figure 2.3 is shown, and one can derive the new radius ( $R_n$ ) and altitude ( $H_n$ ) for disk (n) as shown below, where ( $R_0$ ) is the radius of the circle and the angle ( $\theta$ ) in the elevation plane.

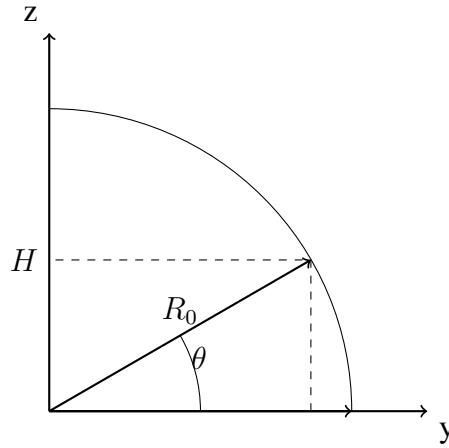


Figure 2.4: Cross section of the first quadrant of the elevation plane, showing two points from the waypoint circles and the angle ( $\theta$ ) between them.

Using trigonometric functions on the figure 2.4 the radius ( $R_n$ ) and the altitudes ( $H_n$ ) of circle (n) can be found as shown in equations 2.17 2.18.

$$R_n = R_0 \cos(\theta_n) \quad (2.17)$$

$$H_n = R_0 \sin(\theta_n) \quad (2.18)$$

It will also be useful to calculate the approximate angle  $\theta$  between two points( $x_1, y_1$ ) and ( $x_2, y_2$ ) on the arc by using equation 2.19.

$$\Delta\theta = \tan^{-1}\left(\frac{z_1}{y_1}\right) - \tan^{-1}\left(\frac{z_2}{y_2}\right) \quad (2.19)$$





# Chapter 3

## System design

This chapter gives an overview of the system architecture before the proposed solution for the design is presented. Since the project combines the common method of antenna measurement in anechoic chambers and using a commercial available multicopter, the system design is based around the integration of all components into an embedded system.

### 3.1 System architecture

For the system architecture figure 3.1 shows how the two subsystems is embedded into one complete system.

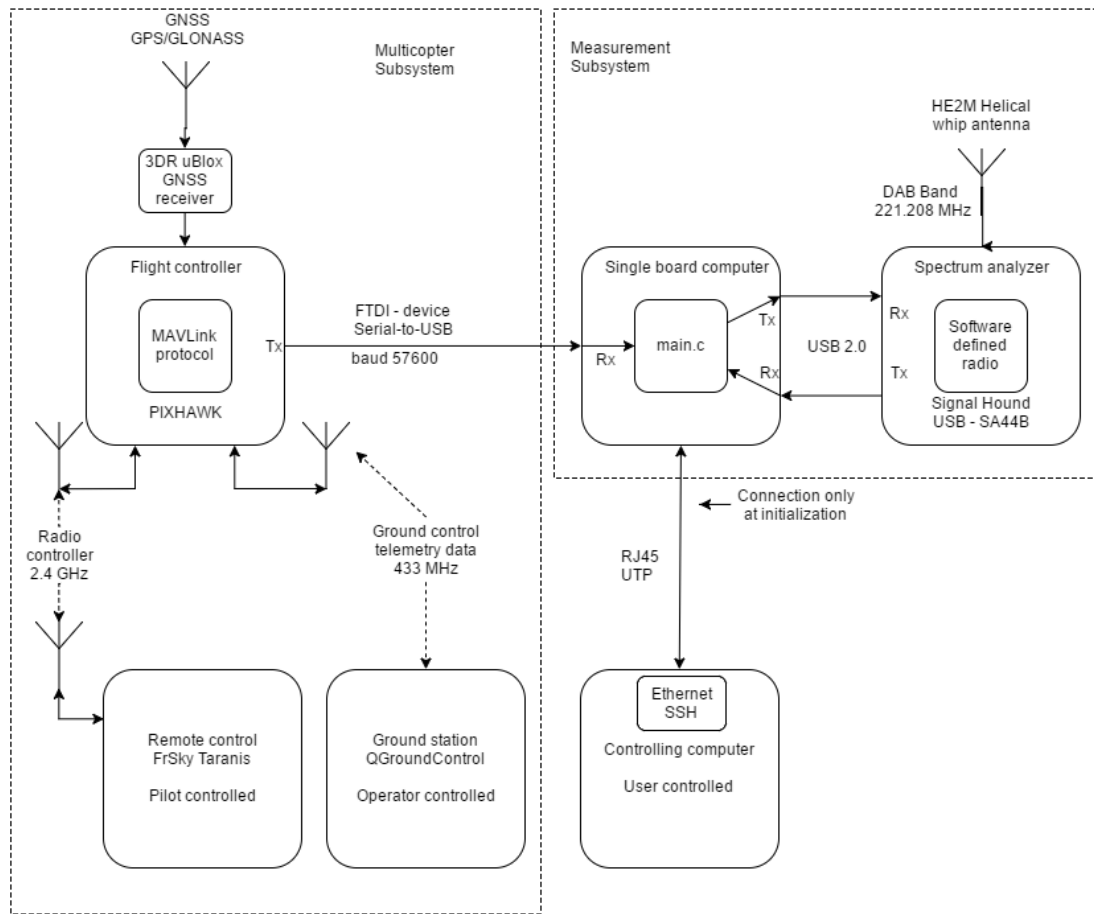


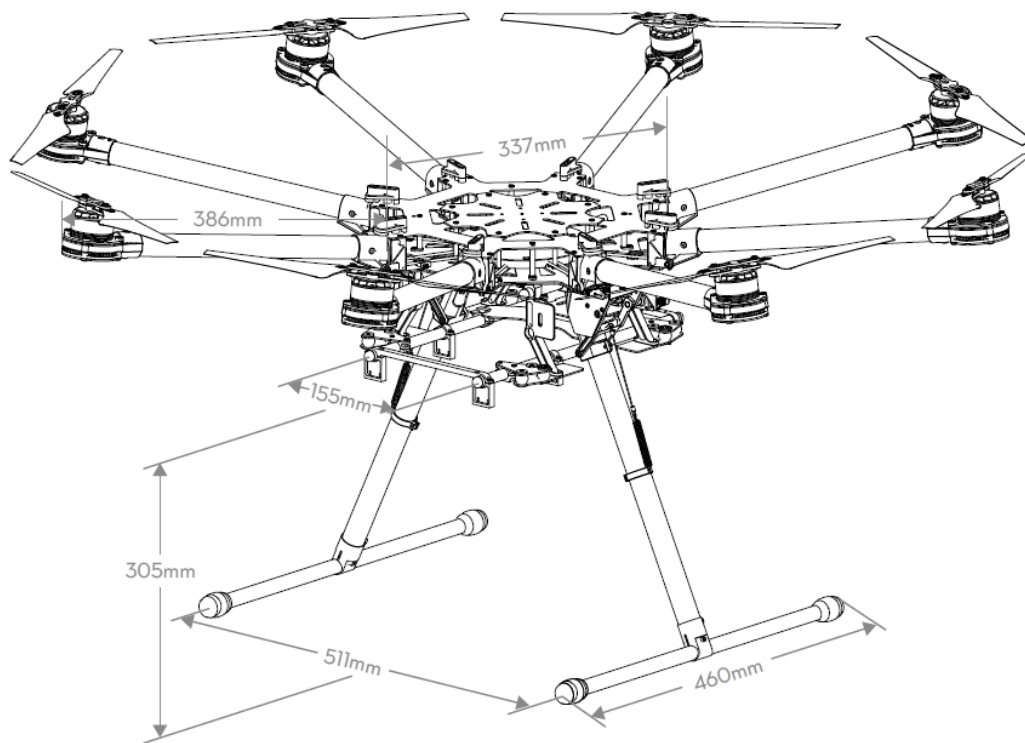
Figure 3.1: Total system overview with the UAV subsystem on the left, and the measurement subsystem communicating with the drone on the right side.

The measurement part of the system, shown to the right in the overview, is a stand alone subsystem with only the serial transmitting link from the flight controller as the connection between the two subsystems. This link is only used to read the MAVLink data broadcast from the flight controller. The Odroid will run the main program for the measurement routine and communicate with the spectrum analyzer using the USB link. When activated the spectrum analyzer gathers the received power measured from the electric field strength through the measuring antenna at the specified frequency. To know where the field strength is sampled in terms of the position the measurements have to be synchronized with the time stamp of the positions logged through the GNSS on the flight controller. This can be achieved through the serial link between the flight controller and the Odroid by reading the MAVLink data stream and synchronize the clocks on the Odroid with the GNSS data. At initialization and before flight a controlling

computer is connected to the Odroid via the ethernet port and using the Linux secure shell (ssh) program to access the Odroid to start the measurement program remotely.

## 3.2 Multicopter

The selected drone used for this project is the DJI S1000+ octocopter [12] with retractable landing gears, which was recommended by the UAV laboratory due to the size and weight of the payload. The multicopter with size specifications is shown in figure 3.2 and with the following system specifications shown in table 3.1.



© 2016 DJI. All Rights Reserved.

Figure 3.2: DJI S1000+ octocopter with size measurements from the user manual [7].

Feature	Value	Notes and conditions
Total Weight	4.4 kg	
Takeoff Weight	6.0 kg to 11.0 kg	
Battery selected	20 Ah	6S LiPo
Max Power Consumption	4 kW	
Hover Power Consumption	1.5 kW	at 9.5 kg takeoff weight
Hover Time	15 min	at 1.5 Ah and 9.5 kg takeoff weight

Table 3.1: Key specifications of the DJI S1000+ octocopter taken from the user manual [7].

The main component in the UAV system is the flight controller of the drone, the Pixhawk PX4 [34], all communication and navigation of the drone is handled by it. The multicopter can be controlled through at least one of the following methods:

1. The flight controller itself can control the multicopter autonomously.
2. Through the ground station by an operator, using MAVLink commands.
3. The operator's remote control as the common way of operating remote controlled vehicles.

### 3.2.1 Global Navigation Satellite System receiver

As shown to the top left in figure 3.1 the GNSS radio receiver of the multicopter subsystem is the 3DR u-blox GNSS receiver [25]. According to the datasheet the NEO-7 u-blox 7 GNSS module [35] is used and has an update rate up to 10 Hz using the GPS mode. This is how often the time stamped positions can be logged, and is set to 1 Hz by default.

## 3.3 Software code

The coded program on the Odroid is the main process to manage and execute the measurements. The programming language is written in C and using Bash script in Linux to perform some system operations and driver module configurations for the measurements.

### 3.3.1 Workflow

The task of the coded program is to ensure that the system gets the software and hardware clocks in sync with the flight controller before it performs the measurements. The program routine is illustrated in a process block diagram in order to create a visual overview of the code shown in the figure 3.3 below.

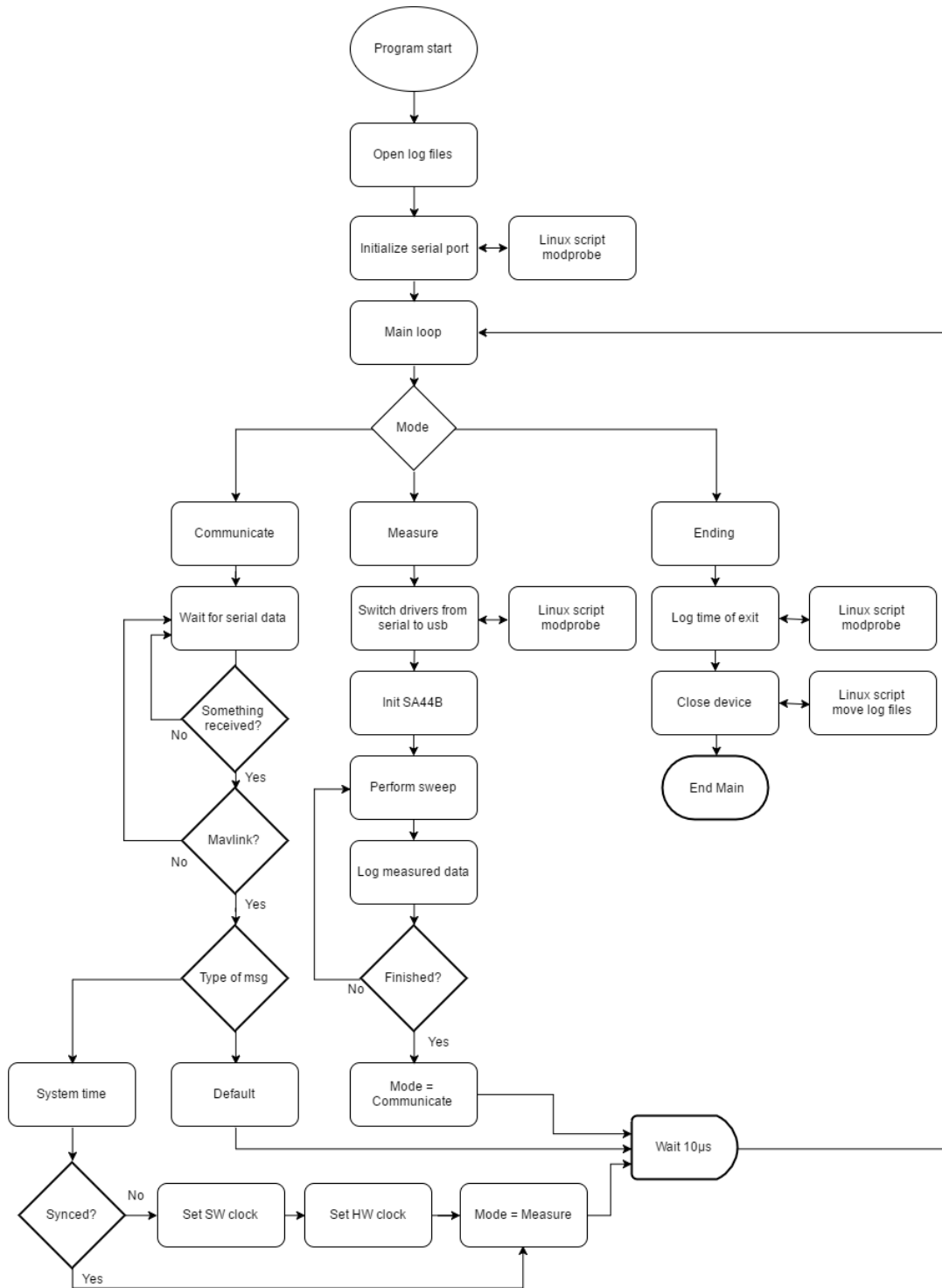


Figure 3.3: Process block diagram of the program code.

The program starts off by creating log files for the events, measurement data and errors that may occur during the execution. Then it configures the serial port of the Odroid using a Bash script to manage the drivers<sup>1</sup> which makes it be able to read data from the FTDI serial to USB converter device. This script will be used whenever the Odroid needs to read from the device, it will also cause the Odroid to be unable to communicate with the attached spectrum analyzer over the USB port.

The program will enter the main loop and select one of three modes, communicate, measure or ending. In communicate mode it tries to read the data broadcasted from the flight controller, when packages is received and confirmed as the MAVLink protocol the system will try to fetch the system time from the GNSS data, if a valid time is received the system will update the hardware and system clock. Then it will enable the measurement to start as the next main branch. In measure mode the spectrum analyzer is initialized with selected frequency ( $f$ ), span ( $\Delta f$ ), resolution bandwidth (RBW), video bandwidth (VBW) and number of samples to be fetched before it is set to measure the electric field strength. When the spectrum analyzer is done sampling the mode is set to ending, which performs a clean closure of the analyzer and writes the logs to time stamped files before exiting the program.

Since the Odroid only receives the broadcasted MAVLink packages from the flight controller a timed measurement will have to be implemented to ensure that the measurements is performed under the whole flight. To know how long time the measurements take, some timing tests have been done and is shown in table 3.2, the settings under the timing was set to  $f = 221.208$  MHz, span = 1000 Hz and RBW = VBW = 4000 Hz.

Number of samples	Time (s)	Time
1	4	
10	4	
100	4.6	
1000	11.7	
10000	82	1 min 22 s
20000	161	2 min 41 s
40000	317	5 min 17 s
80000	631	10 min 31 s
90000	711	11 min 51 s

Table 3.2: Timing test of some selected number of samples executed by the program.

Depending on how long one full flight takes the selected number of samples would have to be chosen near the assumed time in order to sample the whole time.

---

<sup>1</sup>Using 'modprobe' for managing driver modules.

### **3.4 Physical design**

The physical design was using the previous setup from the specialization project [5] as a starting point. Since the equipment is to be embedded on to a multicopter there is some size and weight restrictions that needs to be taken into the design.

### **3.5 Payload**

As mentioned in the introduction chapter the equipment to be used for the measurements are the same as from the project [5]. This includes the Signal Hound [26] USB-SA44B spectrum analyzer and USB-TG124 signal generator, with the Odroid XU4 from Hardkernel [36] and using two DAB configured vehicle antennas together with a flexible helical whip antenna as the payload antenna.

### 3.5.1 Antennas

#### DAB magnetic base antenna

The antenna was bought from Holund Elektronikk AS, from the datasheet [8] the following figure 3.4 shows the length and angle of the antenna, and the specifications is shown in table 3.3.

2 Dimension (Unit: mm)

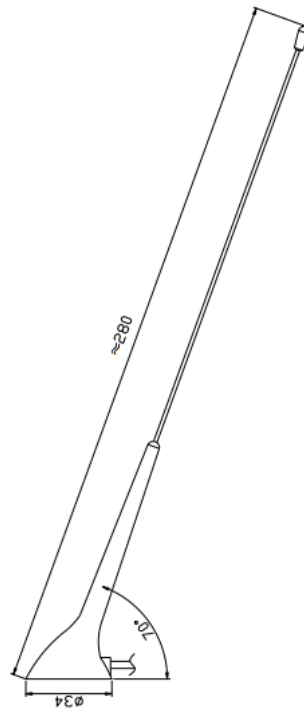


Figure 3.4: DAB magnetic base antenna for vehicles [8].



Type	Passive
Frequency	B III: 174-237 MHz
	L-Band: 1452-1492 MHz
Gain	0 dB
VSWR	$\leq 1.5 : 1$
Impedance	$50 \Omega$
Cable	RG316 4m
Connector	SMB right angle female
Length	280 mm

Table 3.3: Specifications of DAB magnetic base antenna for vehicles. [8]

### Windshield mounted DAB antenna

An antenna with mounting at the inside of the windshield Tiny Audio DAB Antenna AD01 from TT Micro [9], was used for the other type of common vehicle antennas under the measurements. Figure 3.5 shows an illustration of the placement of the antenna and table 3.4 lists the available specifications [37], this antenna is also an active antenna and had to be converted into a passive in order to work as the measurements is set up.

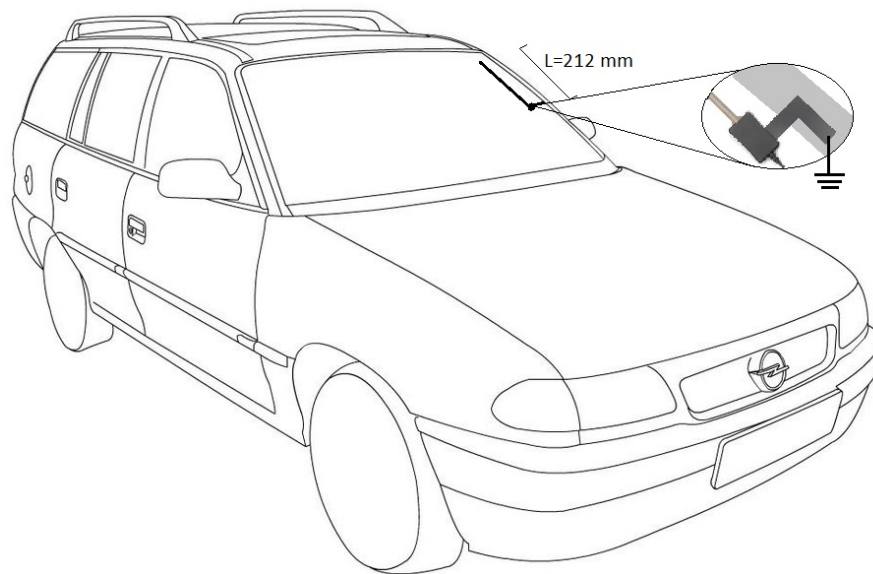


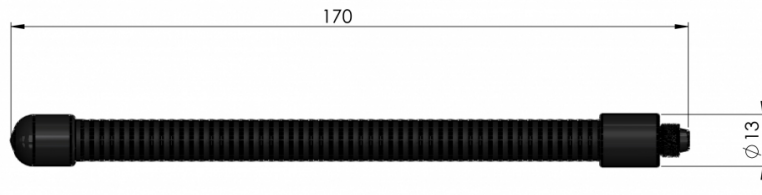
Figure 3.5: DAB windshield mounted active antenna [9] illustrated mounting on the test vehicle Opel Astra G estate [10].

Type	Active (5-28 V, 40 mA phantom)
Frequency	174MHz - 240MHz (Band III)
Gain	N/A
VSWR	N/A
Impedance	Assumed 50 $\Omega$
Cable	3m
Connector	SMB right angle female
Length	212 mm

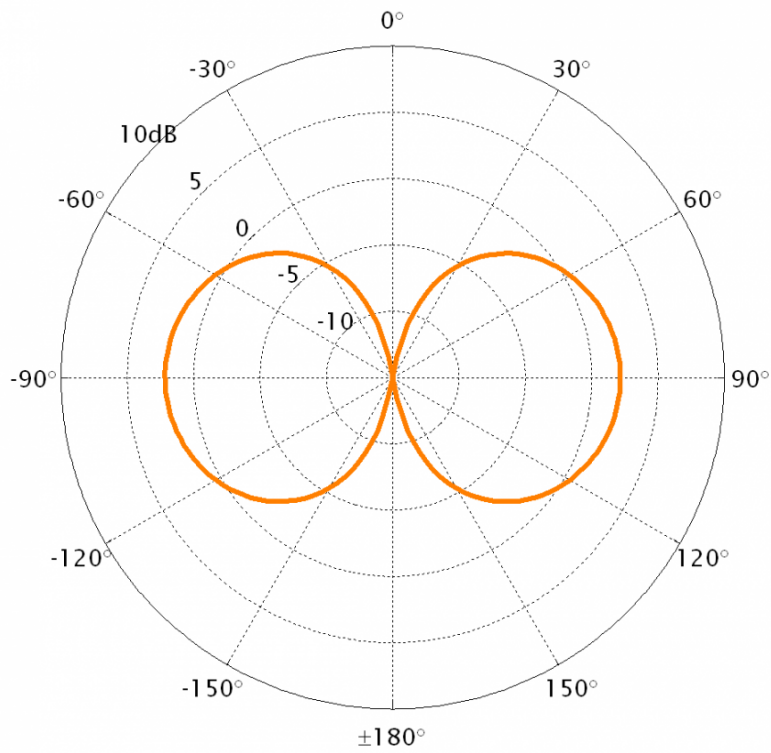
Table 3.4: Specifications of DAB windshield mounted antenna for vehicles [9].

### **Helical whip antenna**

For the payload mounted antenna used as the receiving part of the measurement sub-system a tunable helical whip antenna from SCAN Antenna [11] is used. This antenna works in normal mode and the radiation pattern can be compared with a dipole antenna if a ground plane of sufficient size is present, see figure 3.6a and b for the dimensions and radiation pattern. See the following table 3.5 for the specifications of the antenna.



(a) HE2M Helical whip antenna with dimensions.



(b) Radiation pattern assumed given in the elevation plane.

Figure 3.6: Dimensions and radiation pattern for the HE2M helical whip antenna [11].

Frequency	144-225 MHz (2M BAND)
Gain	2.1 dBi
VSWR	$< 2 @ f_{res}$
Impedance	$50 \Omega$
Connector	FME-female
Cable loss	1.6 dB at 4 m [38]

Table 3.5: Specifications of HE2M helical whip antenna [11].

A cutting table is also included with the antenna, table 3.6 and figure 3.7 shows the lengths given for each frequency range.

Frequency (MHz)	Length (mm)
128-144	No cutting
136-152	153
144-160	147
152-168	141
160-176	135
168-184	128
166-192	123
184-200	118
192-208	113
200-216	109
208-225	105

Table 3.6: Cutting table for the HE2M helical whip antenna.

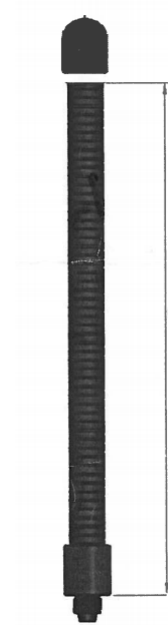


Figure 3.7: Reference length measurement for the cutting length.

For the measurements in the higher elevation angles the measurement data should be corrected with the radiation pattern of the flexible helical whip antenna as shown in figure 3.6, using the table 3.7.

Angle $\theta$	Compensation dB
10	0
20	1
30	2
40	2.1
50	4.6
60	7.1
70	12.1
80	22.1
90	-

Table 3.7: Compensation dB table from the angular dB reduction of the radiation pattern of the flexible helical whip antenna.

### 3.5.2 CAD model

By sketching a layout of the implementation for the measurement subsystem using the computer aided design (CAD) program SolidWorks [39] student edition, the following models as figure 3.8 shows the bottom view of the subsystem.

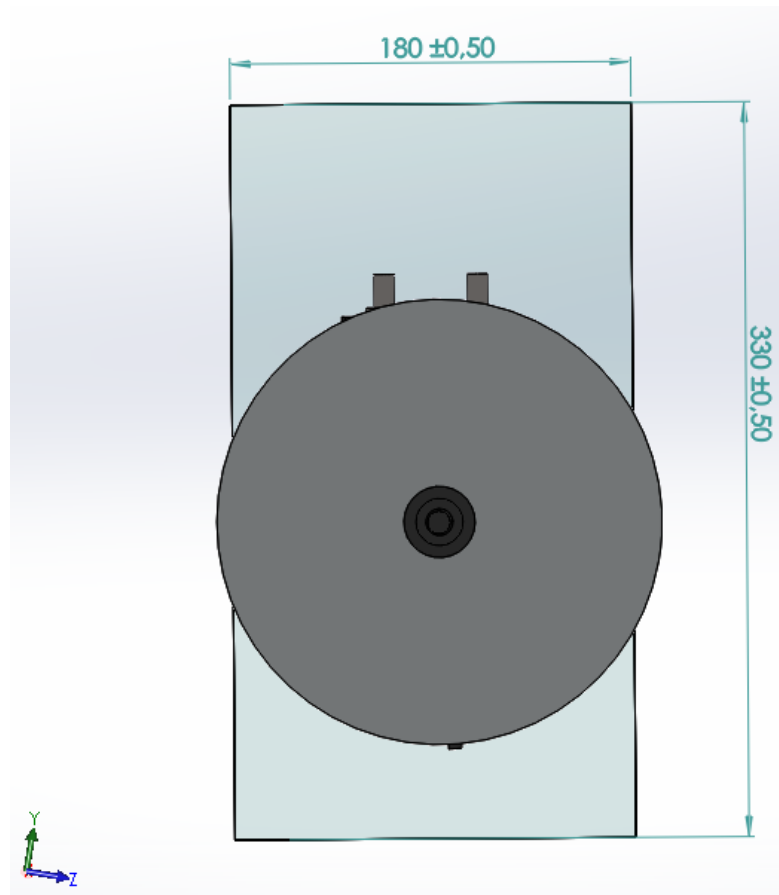


Figure 3.8: Bottom view of the proposed measurement subsystem with dimensions given in mm of the sides.

The subsystem dimensions is designed with the length and width not exceeding the dimensions of the bottom space of the multicopter between the retractable legs as previously shown in figure 3.2. A side view of the subsystem is shown in figure 3.9.

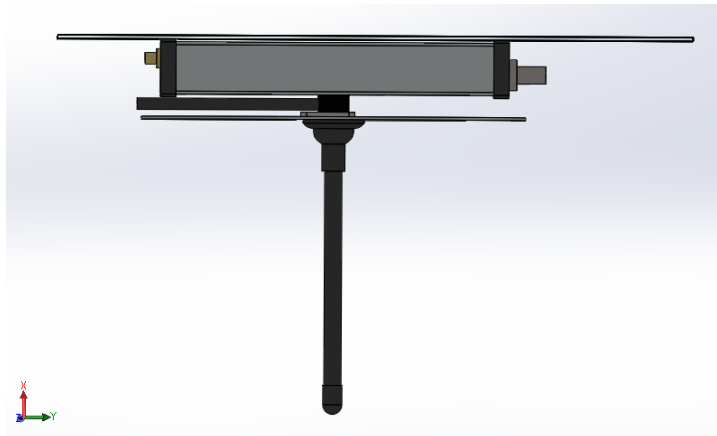


Figure 3.9: Side view of the measurement subsystem with all main components assembled in the correct order, without cables and connectors.

By using the exploded view feature in SolidWorks [39] figure 3.10 shows the whole assembly separated to give a nice overview of how the subsystem is connected together.

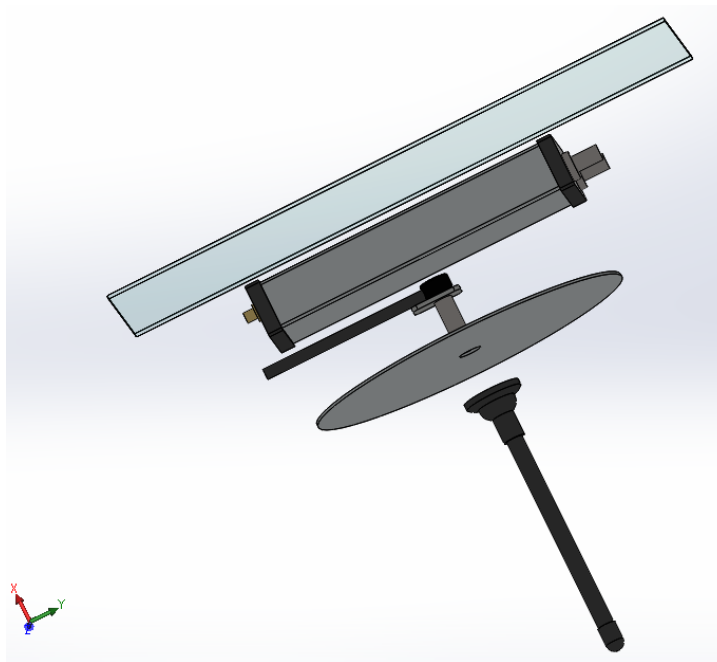


Figure 3.10: An exploded view of the measurement subsystem pointing downwards.

As a final design assembly using the CAD file from the web community GrabCAD [13] the whole system is put together in a full view to see the complete system as it would look after the implementation, this is shown in figure 3.11 below.

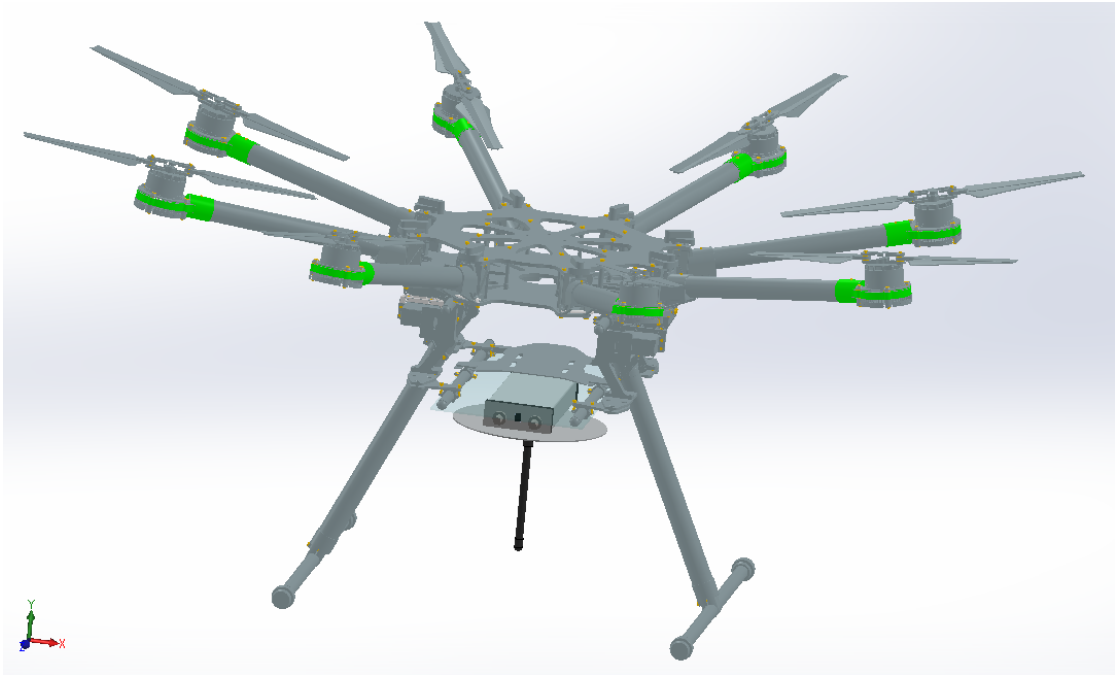


Figure 3.11: A complete illustration of the measurement subsystem assembled onto the mounting bracket of the DJI S1000 [12][13].



# Chapter 4

## Implementation and testing

In this chapter the physical implementation of the measurement system is presented as how it was proposed in the system design chapter. The first section will present how the helical whip antenna used with the spectrum analyzer was tuned into the correct frequency. Then a section showing the realization of the measurement subsystem, before a last section for the measurement testing using the implementation.

### 4.1 Antenna tuning

The helical whip antenna figure 3.6a, bought for this project is when unmodified tuned for 128-140 MHz as shown from table 3.6, which is too low for the DAB frequency band of 174-240 MHz. The target frequency is 221.208 MHz and the antenna needs to be cut so the S11 parameter is the lowest in dB at this frequency for the best match. Figure 4.1 shows the response of the matching s-parameter S11 over the frequency range (100-300) MHz where the antenna is resonant on the frequency 152.853 MHz with -20dB. The antenna tuning is also performed with a ground plane disk of 90 mm radius that will be used under the measurements in such way that the antenna will not receive any interference from the top of the drone downwards, it will also direct the radiation pattern 3.6 downwards due to the reflection from the ground plane disk.

## CHAPTER 4. IMPLEMENTATION AND TESTING

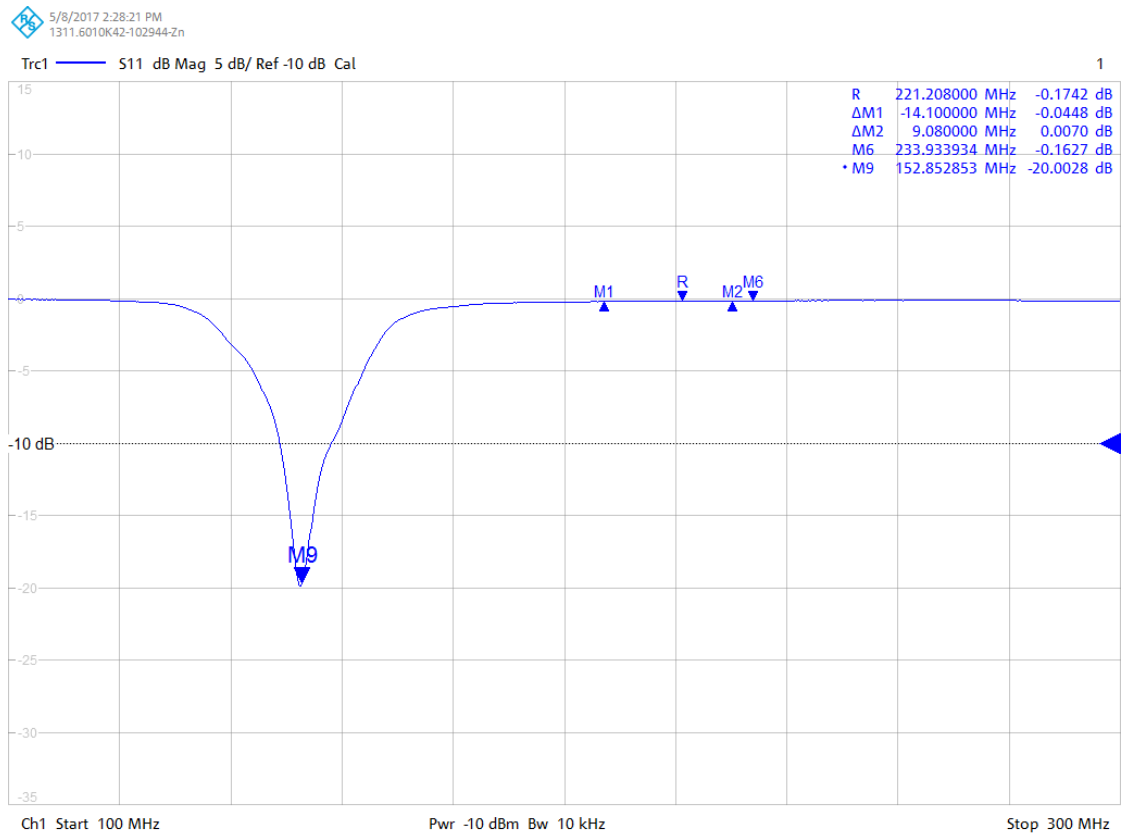


Figure 4.1: The response of S11 over the frequency range (100-300) MHz of the flexible helical whip antenna before tuning, marking the resonance frequency at 152.853 MHz.

From the cutting table 3.6 the antenna is tuned for 128-144 MHz when not cut, to get to the target frequency the length according to the table have to be cut down to the length 105 mm which is in the frequency range 208-225 MHz. Using a cutting tool the antenna were cut down step by step from the table 3.6 to ensure it is not cut too much. The final length ended at 109.53 mm as figure 4.2 shows.

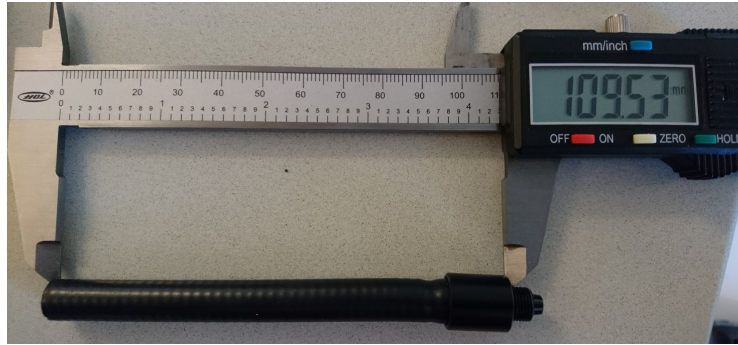
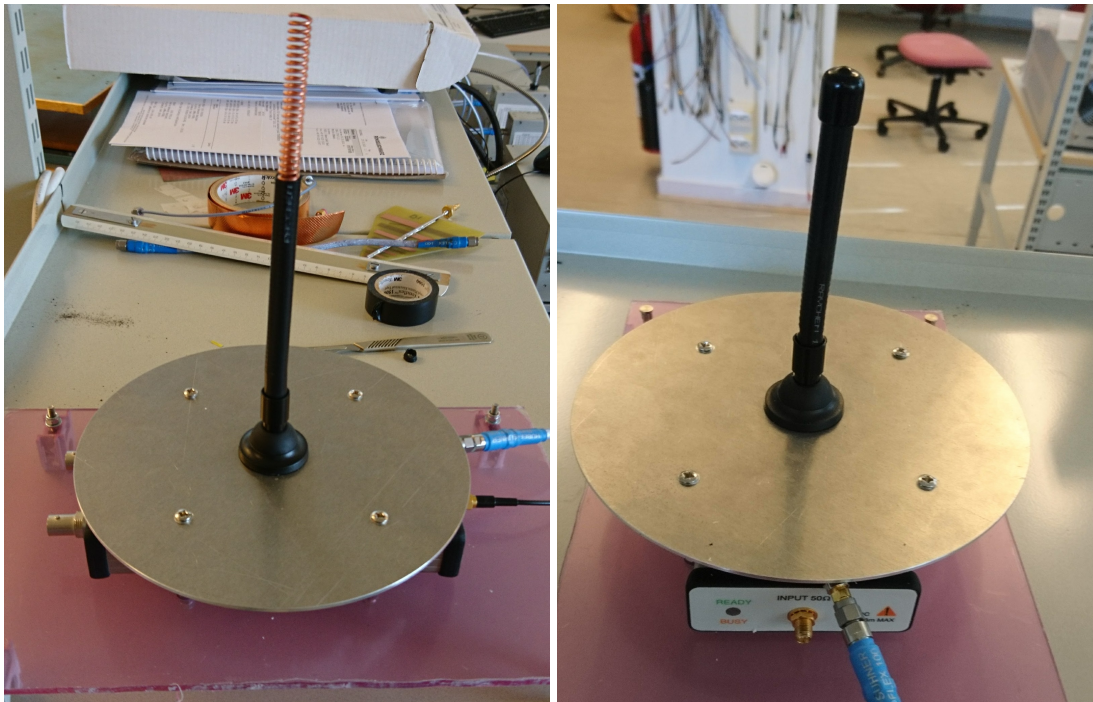


Figure 4.2: Final length of the helical whip antenna.

A before and after cutting picture is shown in figures 4.3a and b, the ground plane disk used for the tuning is also shown in the figures.



(a) Before cut

(b) After cutting to  $L = 109.53$  mm

Figure 4.3: Before and after picture of the tuning process.

At this length the matching s-parameter  $S_{11}$  is as shown in figure 4.4 at  $-7.1$  dB and is the used length for the measurements.

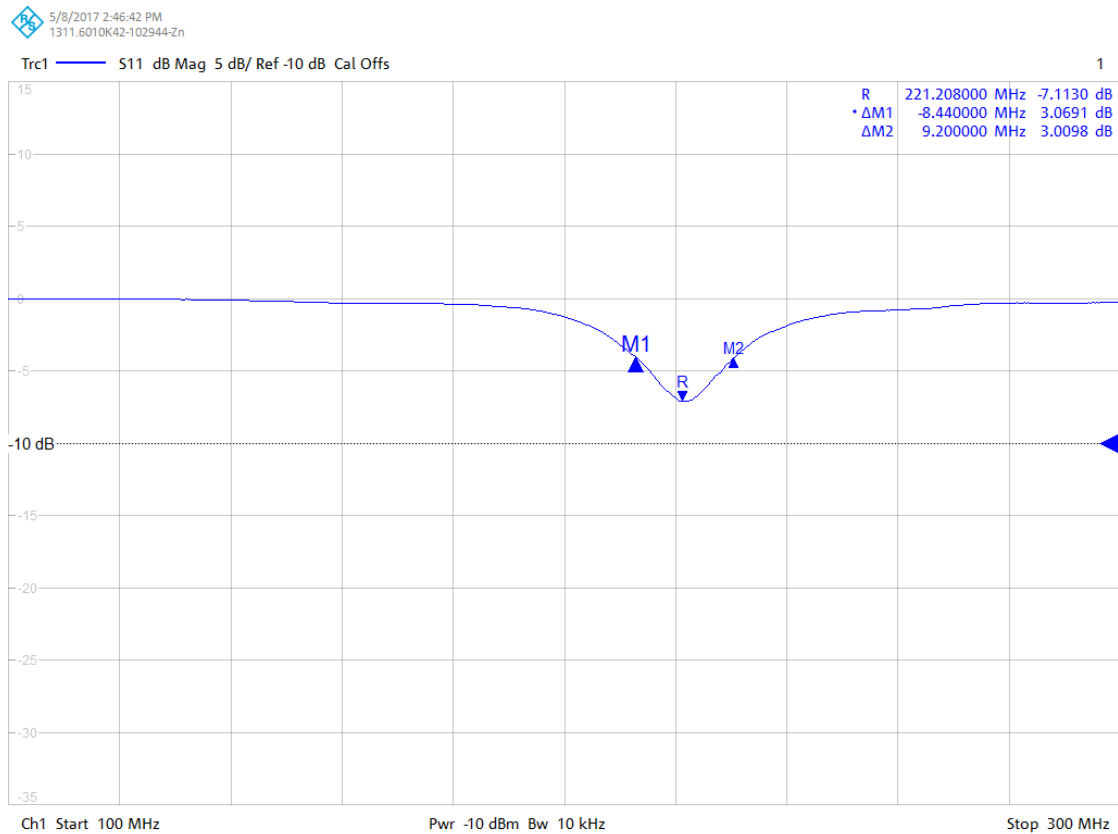


Figure 4.4: The response of S11 over the frequency range (100-300) MHz of the flexible helical whip antenna after tuning, marking the resonance frequency at 221.208 MHz.

The helical whip antenna uses 90° angle FME connector which had to be converted in the other end into a SMA connector.

## 4.2 Construction

The construction process follows the developed system design from chapter 3, the following hardware parts were needed for the assembly.

- One (300 x 300 x 4) mm acrylic sheet plate cut to dimensions (300 x 180) mm as the base for the mounting against the base bars of the multicopter, the length deviates from the planned design with 30 mm shorter than the design, but it had no impact on the fitting onto the multicopter.
- Four long M4 door handle bolts with sleeves for sandwich-mounting the spectrum analyzer and FME connector between the ground plane and base plate.

- Some Styrofoam to hold the spectrum analyzer in place and protect it against scratches.
- Four Castor EC 16 [40] pipe clips fastened in the corners of the base plate, used for snapping on to the base bars of the multicopter base mounting as seen in figure 3.11.
- Some cable zip ties and adhesive mounting bracket for the zip ties, used for fastening the cables.
- Four plastic M3 screws and nuts used for the Odroid to fasten it to the base plate.

After the assembling of the parts the three figures 4.5, 4.6 and 4.7 shows how the complete assembly of the measurement subsystem was, including the testing flight controller.



Figure 4.5: Perspective upside view of the assembly, the antenna is positioned as the back side of the system.

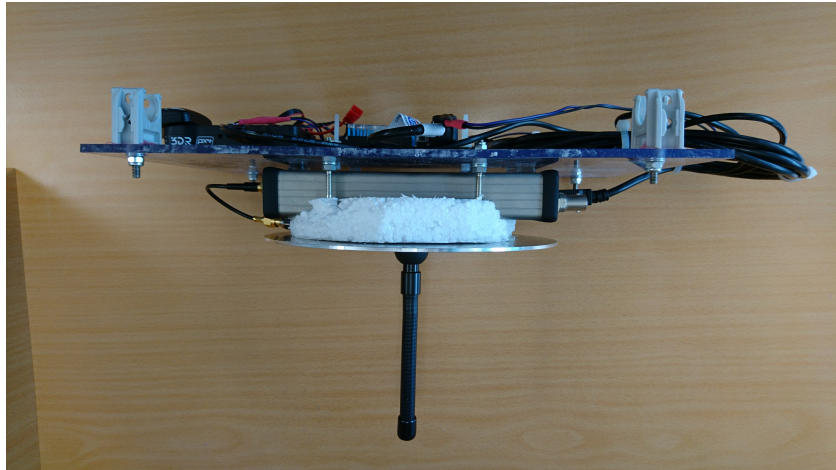


Figure 4.6: Side view of the complete assembly.

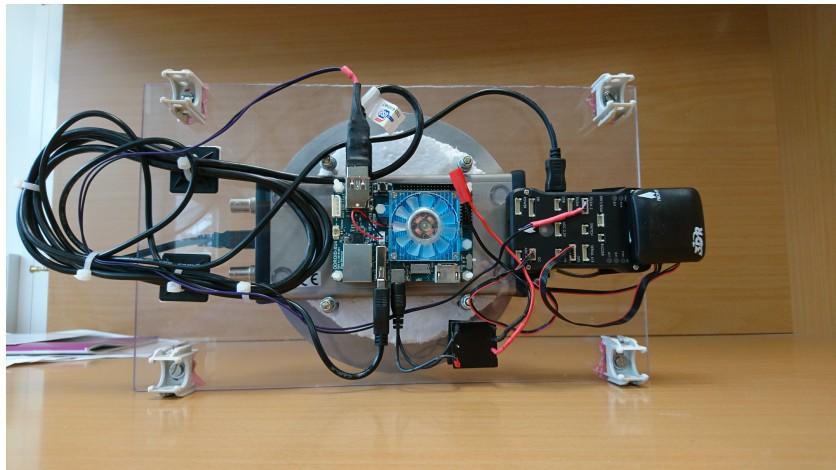


Figure 4.7: A top view of the system connected to the test flight controller to the right.

# Chapter 5

## Measurements

In this chapter the results from the measurements is presented. The measurements were performed only one time on each of the two antennas and is presented in chronological order as how they were measured.

### 5.1 Target frequency

Before the flight the selected frequency for the measurements of 221.208 MHz was verified to not interfering with the DAB channel 11C in the area, this is shown in figure 5.1.

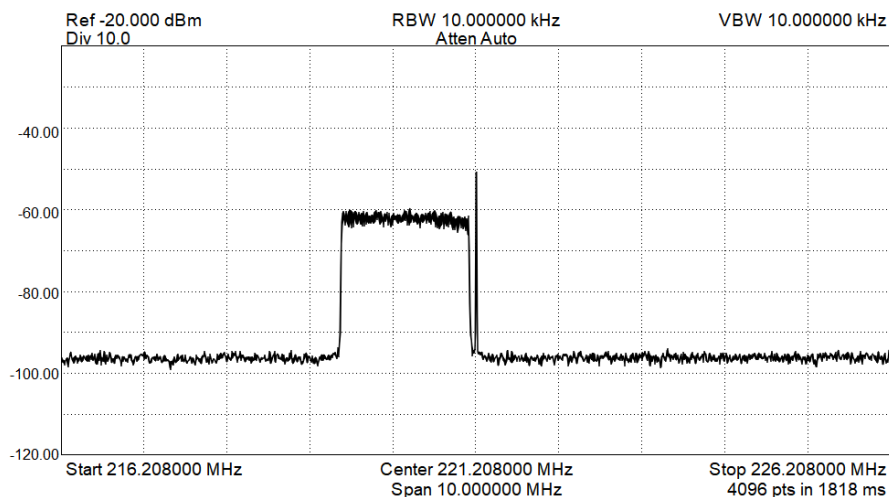


Figure 5.1: A frequency sweep showing the DAB frequency channel 11C for Sør-Trøndelag with the selected frequency for the measurements positioned outside of the channel band.

Since channel 11C ends at frequency 221,120 MHz and the non appearing channel 11D

starts at 221,296 MHz the selected frequency would be right in the middle of the bands. A more detailed view of where the selected frequency is positioned in relation with the channel 11C is shown in figure 5.2

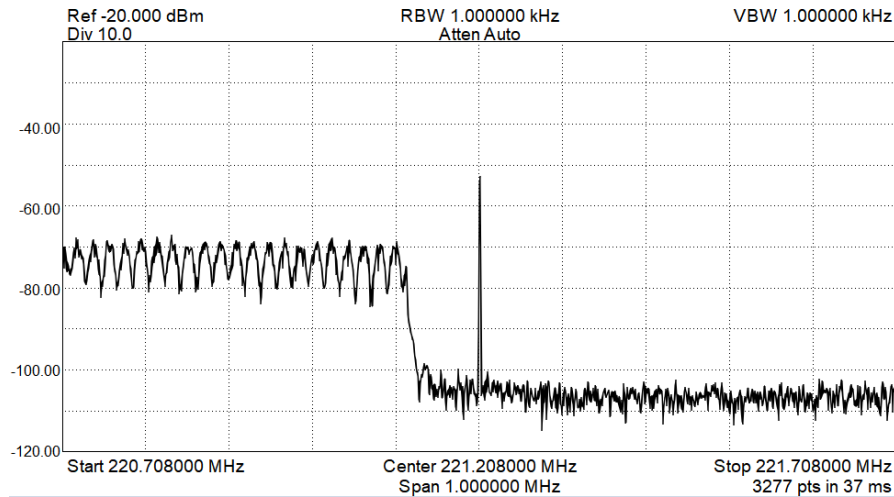


Figure 5.2: A detailed view of the upper part of channel 11C with the selected measurement frequency positioned outside of the band.

The target frequency was powered by the USB-TG124A tracking generator with an amplitude of -12 dBm which is the maximum setting for the generator. The span of the signal is measured to be around 5 kHz.

## 5.2 Drone flight

The weather was cloudy and rainy with the average measured temperature of 12°C given from the vehicle temperature sensor display. The vehicle was positioned in center of the flight path and set as the home position of the multicopter, figure 5.3 shows the angle of the car with the front facing 60° offset from north.



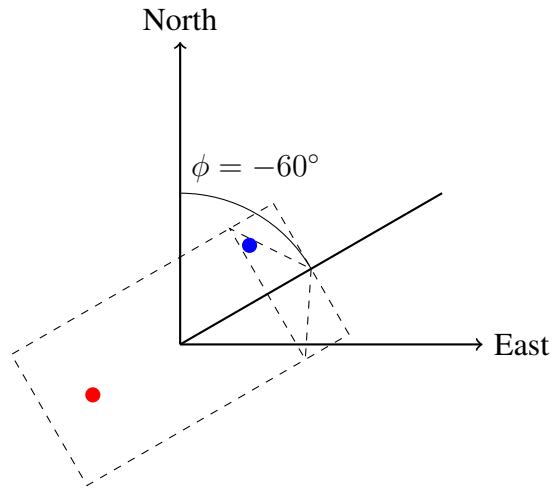


Figure 5.3: Angular placement of the vehicle  $60^\circ$  from the North axis, with dots marking antenna positions, blue windshield mounted and red magnetic base mounted. Home position is set at the center of the vehicle.



Figure 5.4: Picture of the vehicle and location used for the measurements.

The radius for the measurement hemisphere was set to be 20 m and lowest allowed altitude of 3 m, to form an hemisphere elevation angle ( $\theta$ ) was set to be  $10^\circ$  between the measuring disks to get 10 disks of measurements. From the equations 2.17 and 2.18 the radius and altitudes for the flight were calculated and is shown in the table 5.1 below. The mission list for the waypoints is also shown in Appendix A, this list was used for both antennas.

Radius (m)	Altitude (m)
20.0000	3.0000
19.6962	6.4730
18.7939	9.8404
17.3205	13.0000
15.3209	15.8558
12.8558	18.3209
10.0000	20.3205
6.8404	21.7939
3.4730	22.6962
0.0000	23.0000

Table 5.1: Calculated radius and altitudes used for the mission list for the drone under flight.

### 5.2.1 Flights

The first measurement flight was for the magnetic base roof antenna, and the measurements was set to sample 80.000 samples that would yield as from table 3.2 to last about 10 min 31 s as seen from table. Figure 5.5 shows the drone in action under measurements of the magnetic base roof antenna.



Figure 5.5: Picture of the multicopter when measuring the magnetic base roof antenna.

Using the GNSS data logged from the flight, the results from the flight of the first measurement is shown in figure 5.6.

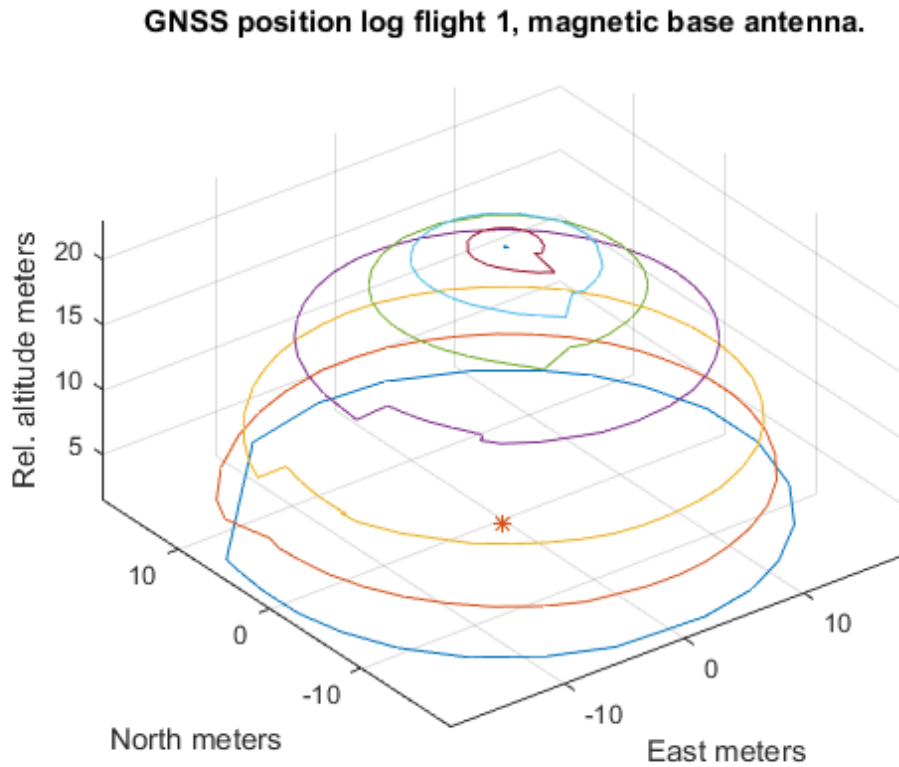


Figure 5.6: GNSS position log data of the flight path when measuring the magnetic base roof mounted antenna, antenna position in red dot and rings at elevations  $\theta = [7^\circ, 16^\circ, 28^\circ, 46^\circ, 59^\circ, 67^\circ, 77^\circ, 87^\circ]$ .

The second flight, measuring the windshield mounted antenna, the samples were set to 90.000 samples (11 min 51 s from table 3.2), and the flight path from the GNSS log is shown in figure 5.7

GNSS position log flight 2, windshield antenna.

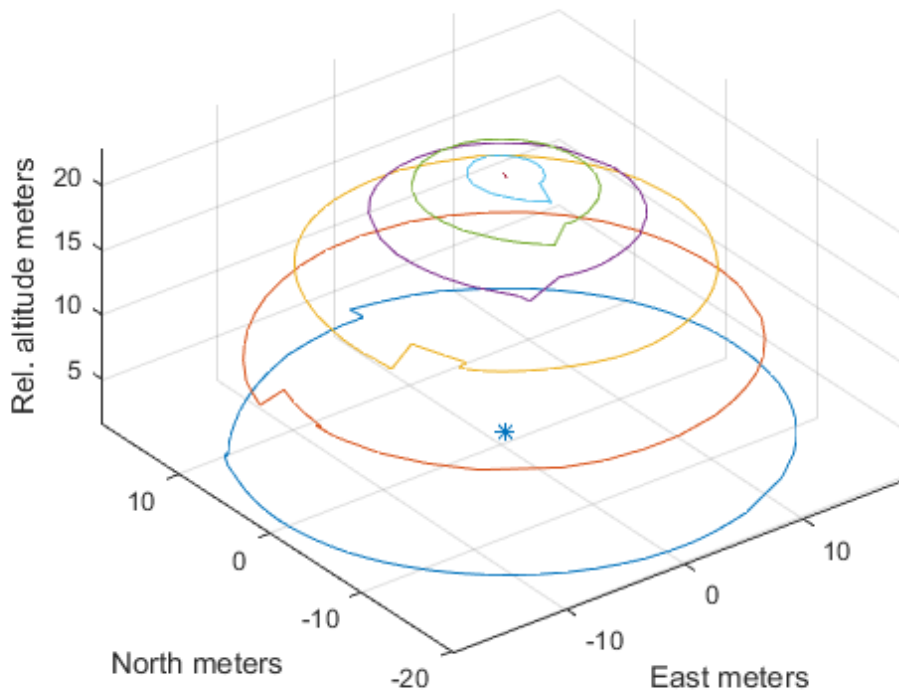


Figure 5.7: GNSS position log data of the second flight path when measuring the windshield mounted antenna, antenna position in blue dot and rings at elevations  $\theta = [8^\circ, 28^\circ, 44^\circ, 58^\circ, 67^\circ, 76^\circ, 87^\circ]$ .

### 5.2.2 Magnetic base roof mounted antenna

The magnetic base antenna were mounted on the roof of the vehicle positioned 0.5 m backwards off the vehicle from the home position which is measured at  $63^\circ 19' 8.689''$  N and  $10^\circ 16' 24.622''$  E, with the height of the car at 1.5 meters. Figure 5.8 shows where the drone was set for the home position on the roof of the vehicle, it also shows the position of the magnetic base antenna.



Figure 5.8: Placement of the magnetic base antenna close to existing antenna on the vehicle, which is disassembled under the measurements. The home position is also shown to be at the middle of the vehicle roof.

Since the vehicle is oriented with the front facing  $60^\circ$  off the north in the East, North and Up (ENU) coordinate system, the antenna position is positioned at the local coordinates  $(-0.25, -0.433, 1.5)$  m, this is shown as the red dot in the figures 5.35.6.

A selected azimuth plot of GNSS position for the magnetic base antenna is shown in figure 5.9 at elevation  $\theta = 28^\circ$ .

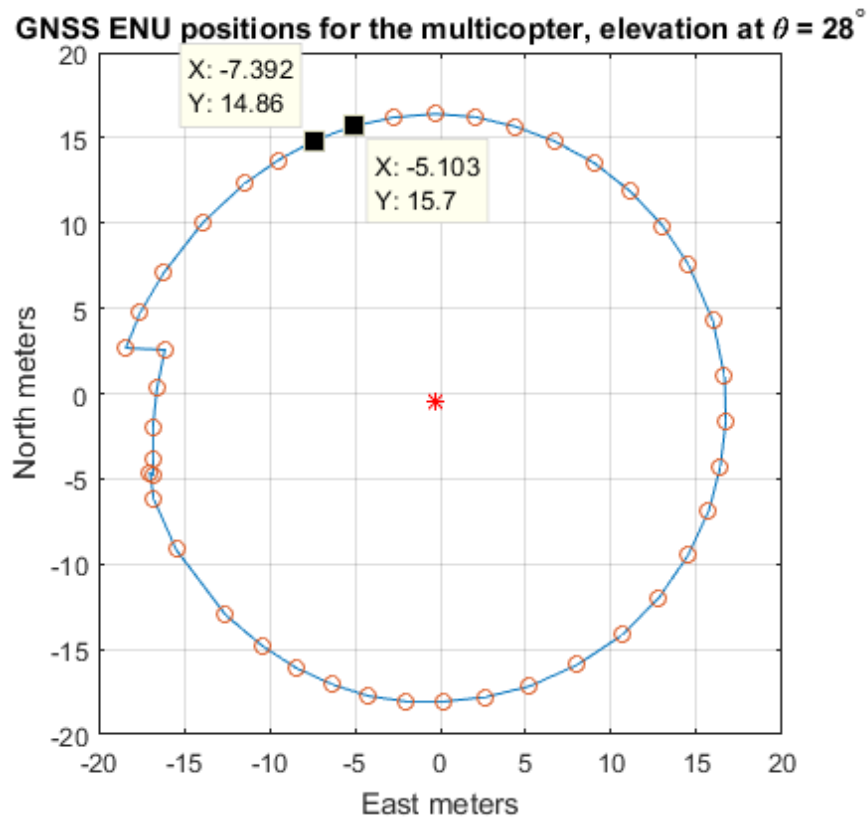


Figure 5.9: GNSS positions of the flight for the magnetic base antenna at elevation angle  $\theta = 28^\circ$ , with the circles marking the sampled position and the antenna position marked as the red dot. Markers shows two subsequent samples used to calculate the angle between them.

The measured received power from the magnetic base antenna from the flight in figure 5.9 is shown in Appendix B in table B.1. The normalized dB radiation pattern is shown in figure 5.10 with the red line as the direction the vehicle were pointing using the GNSS positions from figure 5.10.

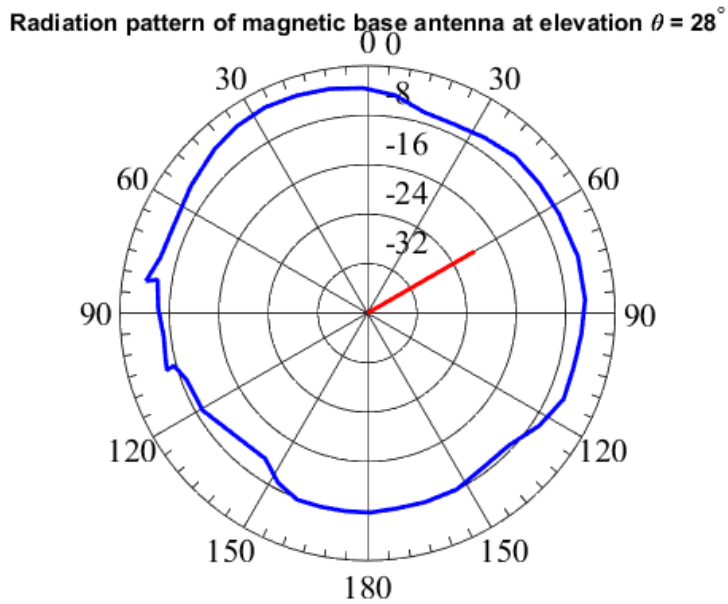


Figure 5.10: A polar diagram of the normalized radiation pattern for the magnetic base antenna, plotted in the azimuth plane at elevation  $\theta = 28^\circ$ , with the red line indicating the angular position of the vehicle pointing at  $60^\circ$ .

From the first flight with the magnetic base antenna, four section of the radiation patterns in the elevation plane is shown as following, starting with figure 5.11 taken at approximately the two azimuth angles ( $\phi = 355^\circ, 175^\circ$ ). The plots are also interpolated with 100 points with the spline method in Matlab in order to present the most probable solution of the radiation pattern. The measured points are shown as the red circles on the curve.

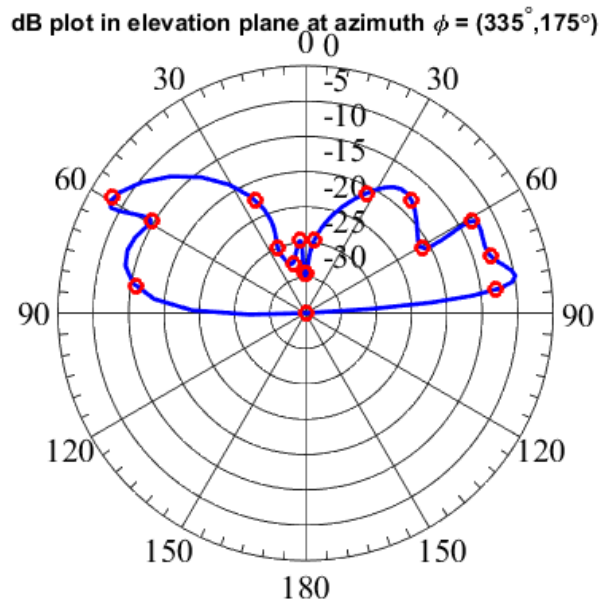


Figure 5.11: Normalized radiation pattern of the magnetic base antenna shown in the elevation plane at azimuth angles ( $\phi = 355^\circ, 175^\circ$ ).

A view of the radiation pattern in the elevation plane from the azimuth angles  $\phi = 50^\circ, 225^\circ$  is shown in figure 5.12.



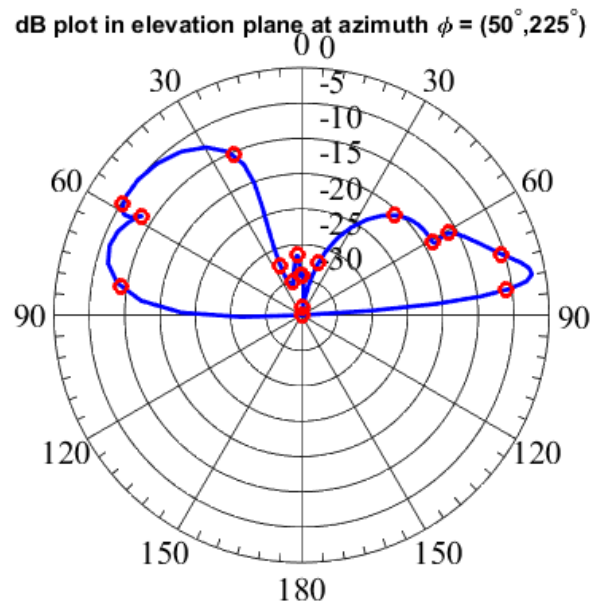


Figure 5.12: Normalized radiation pattern of the magnetic base antenna shown in the elevation plane at azimuth angles ( $\phi = 50^\circ, 225^\circ$ ).

Elevation plane view of the radiation pattern at azimuth angles  $\phi = 85^\circ, 270^\circ$  is shown in figure 5.13.

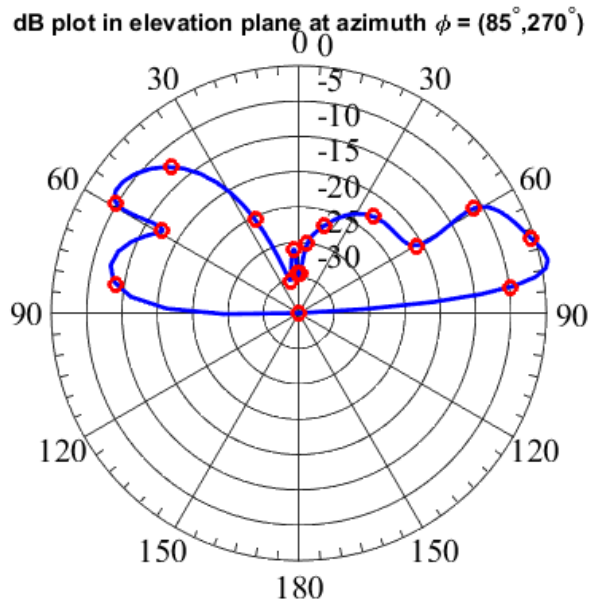


Figure 5.13: Normalized radiation pattern of the magnetic base antenna shown in the elevation plane at azimuth angles ( $\phi = 85^\circ, 270^\circ$ ).

Last elevation plane radiation pattern from the magnetic base antenna at the azimuth angles  $\phi = 145^\circ, 320^\circ$  is shown in figure 5.14.

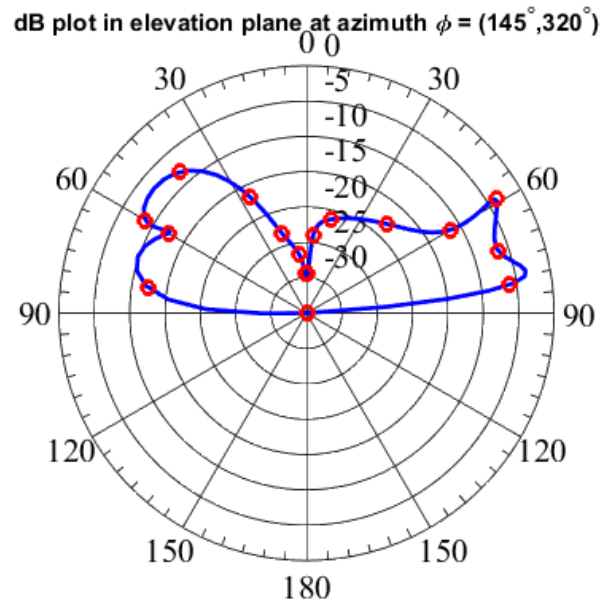


Figure 5.14: Normalized radiation pattern of the magnetic base antenna shown in the elevation plane at azimuth angles ( $\phi = 145^\circ, 320^\circ$ ).

### 5.2.3 Windshield mounted antenna

The windshield mounted antenna were positioned on the drivers side of the vehicle, i.e. the left side of the windshield as the illustration in figure 3.5 shows. Figure 5.15 shows the physical placement of the windshield antenna, with ground connected to the chassis of the vehicle on the window pillar.



Figure 5.15: Placement of the windshield antenna on at the left side of the vehicle windshield grounded to the chassis at the window pillar and positioned from 20 cm to 35 cm down from the roof with an angle of about  $60^\circ$  from the altitude axis.

With the same offset alignment of  $60^\circ$  from North, as with the magnetic base antenna, the local coordinates for the windshield antenna is at (1.1667,1.1667,1.15) m, and is marked as the blue dot in figure 5.16.

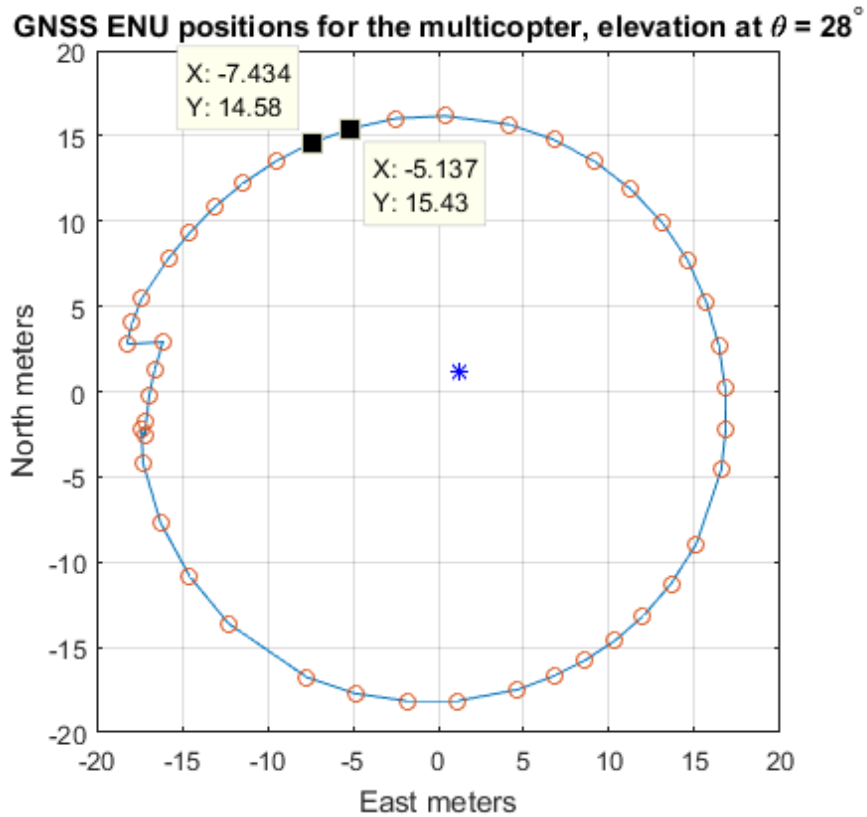


Figure 5.16: GNSS ENU positions of the drone flight path for the windshield antenna at elevation angle  $\theta = 28^\circ$ , with the circles marking the sampled position and the antenna position marked as the red dot. Markers shows two subsequent samples used to calculate the angle between them.

The normalized dB radiation pattern for the windshield mounted antenna is presented in figure 5.17 using the red line for the angular position of the vehicle of  $60^\circ$ .

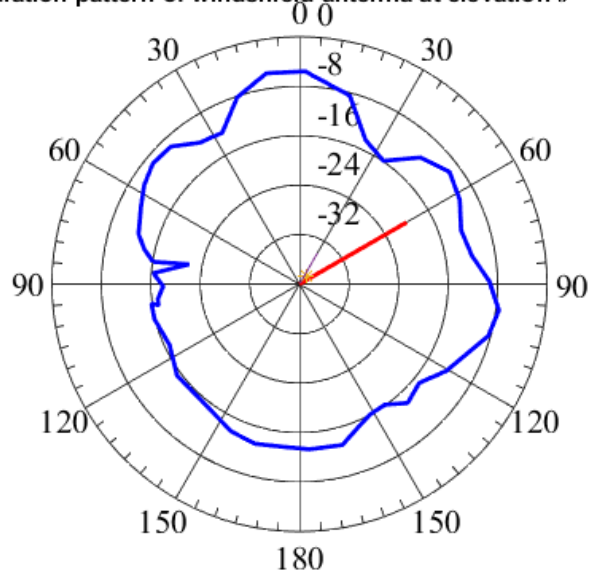
Radiation pattern of windshield antenna at elevation  $\theta = 28^\circ$ .

Figure 5.17: The normalized radiation pattern for the windshield antenna, plotted in the azimuth plane at elevation  $\theta = 28^\circ$ , with the red line indicating the angular position of the vehicle pointing at  $60^\circ$ .

The windshield antenna is also represented with the radiation patterns in sections of the elevation plane using the same azimuth angles as with the magnetic base antenna. Starting with the azimuth angles ( $\phi = 355^\circ, 175^\circ$ ) figure 5.18 shows the radiation pattern in the elevation plane. The results are also interpolated with 100 points using the spline method in Matlab.

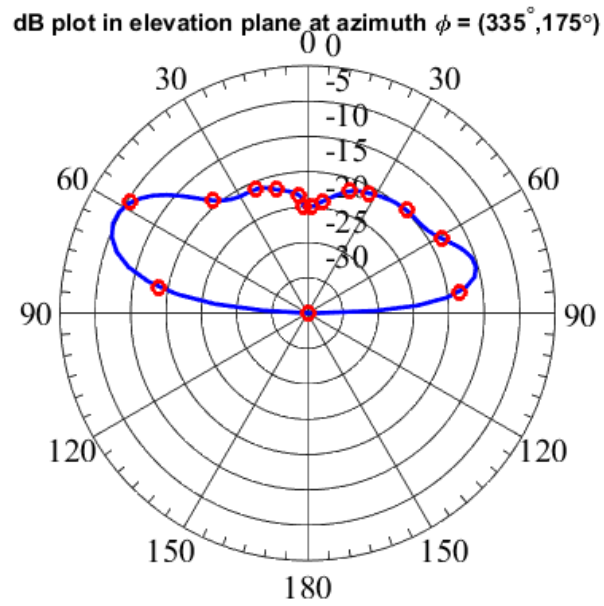


Figure 5.18: Normalized radiation pattern of the windshield antenna shown in the elevation plane at azimuth angles ( $\phi = 355^\circ, 175^\circ$ ).

Second view of the radiation pattern in the elevation pattern at the azimuth angles ( $\phi = 50^\circ, 225^\circ$ ) is shown in figure 5.19.

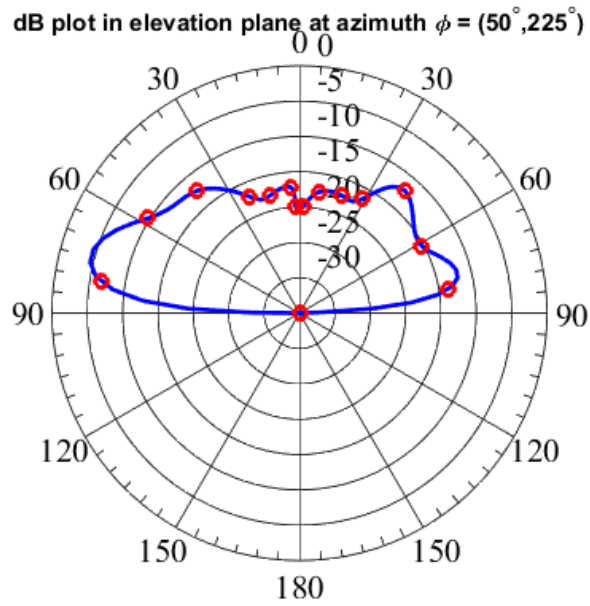


Figure 5.19: Normalized radiation pattern of the windshield antenna shown in the elevation plane at azimuth angles ( $\phi = 50^\circ, 225^\circ$ ).

Third view of the radiation pattern in the elevation pattern at the azimuth angles ( $\phi = 85^\circ, 270^\circ$ ) is presented in figure 5.20.



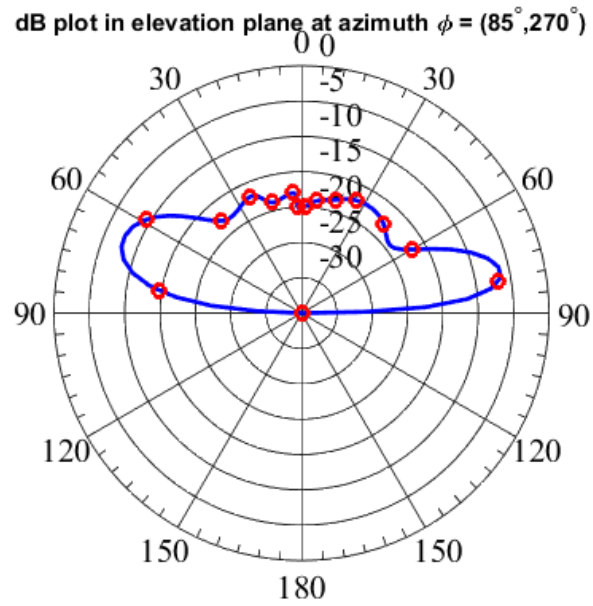


Figure 5.20: Normalized radiation pattern of the windshield antenna shown in the elevation plane at azimuth angles ( $\phi = 85^\circ, 270^\circ$ ).

The fourth and last radiation pattern in the elevation plane is shown in figure 5.21 at the azimuth angles ( $\phi = 145^\circ, 320^\circ$ ).

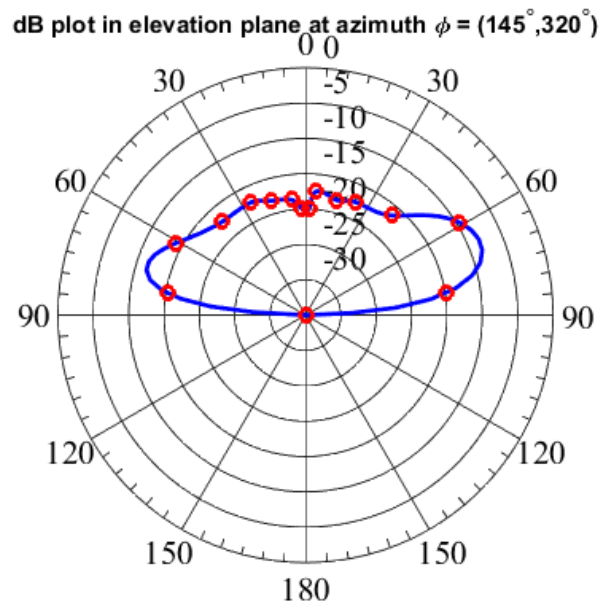


Figure 5.21: Normalized radiation pattern of the windshield antenna shown in the elevation plane at azimuth angles ( $\phi = 145^\circ, 320^\circ$ ).

# Chapter 6

## Data analysis and verification

In this chapter the discussion of the project results is presented, first a section discussing the method used for the thesis, then the measurement results is analyzed, compared and discussed to verify if the data is consistent with the calculations and predictions. A section dedicated to error sources is also presented before the last section of future work is explained.

### 6.1 Method

Since the main goal of this project was to explore the ability to use a drone in antenna measurements the scientific method was approached in the best manner as possible. The problem was first analyzed and some solutions were sketched for the system design. The project is a typical hands-on project with no given restriction of the chosen solution other than keeping the limits to use the previous equipment and drone selected by the UAV laboratory. All materials used in addition to the equipment is commonly available at any hardware store in Norway at a reasonable price, and were selected due to keeping the solution elegant and simple without big expenses.

The method is however based around creating an embedded system prototype that has to perform coordinated measurements with another system, it has some room for improvement that can be seen at the end of the project. The selected multicopter should have been chosen earlier in the project to get the dimensions for the hardware parts of the measurement subsystem early on. This is caused by the uncertainty of how the system is best solved before it has been tested and can only be improved by experience. Also, because of the availability of the drone and operator had to be timed with the development of the measurement subsystem it caused some delays and the measurements were only performed once in one day, and would be the major improvement factor for the project to perform some more measurements to tune the system into a more efficient and accurate measuring equipment.

## 6.2 Measurement results

Since the measurements were performed one time on each of the antennas on the vehicle, the results from the measurements cannot be compared with other flight measurements of the same antenna and would have to be relative compared with each other. The results can be analyzed and discussed in how the resolution and accuracy is from the graphically represented data plots in Matlab.

### 6.2.1 Resolution and accuracy

Looking at the resolution of the measurements to determine the accuracy of the antenna measurements the antennas are discussed separately before comparing them together.

#### Magnetic base antenna

For the first flight the results of the magnetic base antenna as presented in the measurements chapter, starting with the GNSS positions shown in figure 5.9 the sampled points marked as the circles shows some unevenly sampling that can cause a decrease of the accuracy of the measurements. By calculating the angle ( $\phi$ ) between the two markers, the angle is using equation 2.19 with  $\phi$  angles and xy positions, the angle is  $\Delta\phi = 8.44^\circ$ . This gives roughly an arc length of 2.36 m at 16 m radius at this elevation angle, which is a little rough spacing and could have been smaller to get the details a little better in the radiation pattern in the azimuth plane as figure 5.10 shows. This could have been solved by setting a higher sampling rate of the GNSS receiver on the drone.

Looking at the radiation pattern in the elevation plane it shows that without the interpolation the results would not have been as smooth as it is shown in the figures 5.11, 5.12, 5.13 and 5.14. The plots have only 15 available points (with two samples repeating at  $\theta = 90^\circ$  to connect the plot in one continuous path) as the circles in figure 5.11 shows. Using the mission list in Appendix A the multicopter should have produced ten GNSS position disks from the measurements, but have somehow skipped a few of the altitudes at angles  $\theta = 40^\circ$  and  $60^\circ$ . A solution for this problem would have to make a new mission list with a flight path that flies in the elevation plane at a selected start and stop azimuth angle to get more samples at a much closer altitude interval.

To control the measurements the use of Friis' transmission equation 2.16 can verify if the received power is correct. From figure 5.10 the measurements is performed in an elevation angle  $\theta = 28^\circ$  which yields an added compensated dB from table 3.7 about 2 dB on the measurements. Using the table B.1 in Appendix B from the measurements and taking the point at  $\phi = 62, 6^\circ$  where the received power is -61,7 dBm, assuming the polarization loss factor is 0 dB since at this angle the drone is in right in front of the

vehicle and the polarization would be the same. Using Friis' transmission equation 2.16 shows that the expected received power would be -55.5 dBm, when transmitted power is -12 dBm, transmitter gain is 0 dB, receiver gain is 2 dB, at frequency 221.208 MHz, using the radius of 20 m, from figure 5.9 and including the RG-316 cable loss [38] of -1.6 dB. This is 6.2 dB less than actual measured value and if including some expected losses as connection loss, somewhat polarization loss, matching loss or even the weather could have some impact on the measurement, all of these could add up to the expected result. Looking at the maximum measured value for the flight the result is -56.6 dBm at azimuth angle  $\phi = 1.70^\circ$ , elevation angle  $\theta = 17.4^\circ$  and radius 19.8 m, which is between two circles. This result is more coherent with the expected value from Friis' transmission equation and is just off with about 1.1 dB that can be some loss in the transmission.

### Windshield antenna

The GNSS position results from the windshield antenna shown in figure 5.16 is almost equal to the magnetic base antenna positions and shows that the drone samples the GNSS data in a consistent manner. The samples are also not fully evenly spaced and using the same marker positions the angle ( $\phi$ ) between them, using equation 2.19, is  $\Delta\phi = 8.60^\circ$ . This angle gives an arc length of 2.40 m at the radius of 16 m for this elevation angle. These results are also a little too rough and could have been sampled faster to get a smoother result of the radiation pattern, this is also solvable by setting the sample rate of the GNSS receiver of the multicopter to a higher rate.

Analyzing the measurements using Friis' transmission equation from equation 2.16 with the same values as for the magnetic base antenna but with a cable loss estimated to 1.2 dB (3 m) [38] and the transmitter antenna gain of 0 dB. Using the same point of azimuth angle ( $\phi = 62.3^\circ$ ) with the radius of 20 m, the received power from the measurements in the table B.2 in Appendix B is measured to -89.6 dBm. Comparing the result with Friis' transmission equation 2.16, the expected received power would be -56.56 dBm, which is 33 dB in difference with the measured results.

A possible reason for this huge difference could be that when changing the transmitting antennas, a confusion occurred and the power setting for the tracking generator may have been set to -30 dBm. If this is the case, using the Friis' transmission equation with this value as the transmitting power the expected received power would be -74.56 dBm, and taking the maximum received power from the flight the value is -78.84 dBm, which is at position azimuth angle  $\phi = 58.4^\circ$ , elevation angle  $\theta = 31.4^\circ$  and radius 19.3 m that is presumable in between two circles. Also, this value is more likely to be coherent with Friis' transmission equation and the value is off by 4.28 dB that can be because of the simple conversion of the active to passive antenna modification causing a mismatch

with the reflection coefficient  $\Gamma$ . The antenna were grounded with the adhesive ground pad to the metal chassis part of the pillar on the drivers side and it may cause some bad connection due to the temporarily solution as shown in figure 5.15.

### 6.2.2 Comparison

By comparing the two antennas it can be determined which of the measurements gives the best radiation patterns for DAB radio reception in vehicles. Often the windshield antennas are of the active antenna types and this could be a clue that the reception may be weaker for these and therefore needs the amplification to function better.

Taking the two radiation patterns in the elevation plane at azimuth angles ( $50^\circ$ ,  $225^\circ$ ) in figure 5.12 for the magnetic base antenna and figure 5.19 for the windshield antenna. These radiation patterns is almost taken when viewing the vehicle from the side, with the left side ( $-90^\circ$ ) representing the front of the vehicle, and the right side ( $+90^\circ$ ) as the back of the vehicle. In terms of directivity and gain, shows that using the sampled values with interpolation in Matlab, the magnetic base antenna 5.12 has a bigger main lobe facing forward of the vehicle than the windshield mounted antenna 5.19. It also looks like the windshield mounted antenna have a more oval form of radiation pattern than the magnetic base antenna, which is probably due to the angle the antenna is mounted in the windshield, which is pointing more upwards than the magnetic base roof mounted antenna. Also, the roof antenna is a whip antenna that typically has an omnidirectional radiation pattern as with dipole antennas, with a zero radiation point pointing upwards along the z-axis as seen in the radiation pattern 5.12. It also seems that with the roof mounted antenna, the vehicle roof works as a reflector and directing the radiation pattern more forward than backwards. Together with the angle of the antenna, the main lobe is much bigger facing forwards of the vehicle, which gets reduced on the sides as seen in figure 5.11 and figure 5.13.

Since the measurements are a little rough using the interpolation function on the measurements in Matlab helps showing the most probable pattern based off the measurement data. Taking the figures of the radiation pattern in the elevation plane into account it looks promising of what to expect of these types of antennas. Typically the radio broadcast from the radio towers comes in an downwards angle towards the vehicle and shown by the elevation plane radiation pattern for both antennas, it would be likely that the directivity is pointed a little upwards to maximize the gain of the reception.

## 6.3 Error sources and problems

Since the measurements were only done once, it can be considered as an error source for the testing part of the project. By looking at the first flight when measuring the magnetic base roof antenna, using figure 5.6 and compare it with the mission list in Appendix A in table A.1. This shows that something went wrong with the flight path of the drone at the altitude 13 m, between the third and fourth a circle is missing and at altitude 18 m, between fourth and fifth a circle is missing. This happened also with the windshield mounted antenna. Looking at the figure 5.7 of the second flight there is missing three circles, between the first and second circle at altitude 6 m and at the same two altitudes as with the first flight, the 13 m and 18 m circle.

The cause of these problems seems to lay within the UAV system, probably because of the altitude measurements in the drone is using barometric pressure to determine the altitude and it can have some errors due to this. A solution would be to use a better form of altitude determination, as the research [41] did with a motorized total station.

Another error source is the data synchronization since the measurement subsystem was tested and verified working against a flight controller of the same type as used under flight, the subsystem did not work with the drone flight controller of unknown reasons. This ended in using the working flight controller with the subsystem to be able of getting the system clock and hardware clock synchronized with the GNSS UTC time, which is assumed to be equal to the time received on the drone flight controller when logging the positions. The errors should not be large since the sampling is done at about 1 Hz by the GNSS receiver of the multicopter and the received power sampling is about 125 samples/s, which is read and calculated from the received power data log.

### 6.3.1 Interference

The surveying frequency plot in figure 5.2 from the results shows that the target frequency 221.208 MHz lays just outside the channel 11C band. This proves that the selected frequency is not causing any interference at channel 11C and it also shows that there is no interference on the selected frequency coming from any other sources that may affect the measurements.

### 6.3.2 Software problems

The communication between the Odroid XU4 and the Pixhawk PX4 had some problems due to some driver modules for the USB-to-serial converter device not being set up correctly by the Ubuntu operating system. The SA44B connects to the Odroid XU4 board

via one of the USB 3.0 ports, following the instruction procedure from the Signal Hound API, the driver module `ftdi_sio` has to be disabled using the command `sudo modprobe -r ftdi_sio` in the Linux terminal in order to communicate with the spectrum analyzer. This however creates a new problem when using the USB-to-serial device which connects the flight controller to the Odroid. This device requires the `ftdi_sio` driver module to be activated through the command `sudo modprobe ftdi_sio` in the terminal.

This problem could probably have been solved by using the RS232 serial port on the Odroid, but was not attempted due to the working solution. To implement the driver module switching routine inside the program code, two Linux bash scripts were made and set to be executed inside the code via the call command `'system("script name")'` implemented in the C language.

### 6.4 Improvements and future work

As it seems from the results the main problem of the project is the UAV system, where the GNSS receiver system should be improved to get better accuracy in the measurements and radiation pattern representation. This problem seems to be the same as with the specialization project [5] and should be considered a major improvement factor for the project.

Another improvement for the project would be to use Matlab in creating a fully 3D radiation pattern for the antennas to further represent how the radiation pattern is. Also, it would be interesting to test the system using other antennas at other frequencies, specially at higher frequencies, to see if there is some problems arising with the measurements because of some type of interference from the UAV system or other sources.

Taking the discussion and improvements into account a list of future work is listed as following that can be used to improve the measurements.

1. Use or develop a more accurate GNSS receiver system and altitude measurement.
2. Investigate the communication problem with the multicopter flight controller with the measurement subsystem when all devices is connected properly.
3. Fly again using a closer sampling for the GNSS positions.
4. Develop a routine in Matlab to be able of representing the radiation patterns in three-dimensional figures.
5. Measure and determine the potential interference that the drone produces using an anechoic chamber.
6. Measure antennas for higher frequency and compare it with an anechoic chamber measurement to see how well the drone measurements performs.



# Chapter 7

## Conclusion

In the concluding part of this thesis the problem description states that the task is to develop, implement and test a method of measuring the radiation pattern for one or more common type of DAB antennas mounted on a vehicle using a drone.

This thesis presents a solution for the problem described and has been completed by designing and constructing a measurement system and measuring the electric field strength of two types of DAB antennas for vehicles, one roof mounted and one windshield mounted. The results show that the resolution of the radiation patterns is not as good as wanted, but readable to indicate the probable direction of the radiation lobes.

Overall the measurement system needs some improvement, especially for the GNSS position logging. It would also need some more testing using other types of antennas and frequencies to fully qualify the system for all types of antenna measurements. Also, a better representation of the radiation patterns in three-dimensions would greatly increase the readability of the antenna characterization.



# Bibliography

- [1] LS telcom Group. News. *Antenna RF measurements with a miniature helicopter*, September 2012. <http://www.hamradioweb.org/forums/attachment.php?attachmentid=15272&d=1446894469>, Accessed:20/05/2017.
- [2] Kirt Blattenberger. Drone-Based Field Measurement System (dB-FMS), 2014. <http://www.rfcafe.com/miscellany/homepage-archive/2014/Drone-Based-Field-Measurement-System.htm>, Accessed:26/05/2017.
- [3] Jason Schreiber. Full antenna pattern reconstitution of broadcast systems using unmanned aerial vehicles. *Innovative Drone Solutions*, 2015. <https://www.silvertone.com.au/sites/default/files/attachements/Antenna%20Reconstitution%20Brochure.pdf>, Accessed:20/05/2017.
- [4] Norwegian Communications Authority. Test av DAB antenner og mottakere for bil, måleresultater. *Nkom*, June 2016. [https://www.nkom.no/fritid/digital-radio/digital-radio/test-av-dab-sendere/\\_attachment/24204?\\_ts=155531ec44d](https://www.nkom.no/fritid/digital-radio/digital-radio/test-av-dab-sendere/_attachment/24204?_ts=155531ec44d). Accessed:10/02/2017.
- [5] Yngve Tandberg. *Antenna measurements using drones (Pre-flight) specialization project*. Norwegian University of Science and Technology, 2016.
- [6] Lorenz Meier. Mavlink micro air vehicle communication protocol. <http://qgroundcontrol.org/mavlink/start>, 2009. Accessed:10/05/2017.
- [7] DJI. Spreading wings s1000+ user manual v1.4 2016.01. <http://www.dji.com/spreading-wings-s1000-plus/info#downloads>, Jan 2016. Accessed:12/06/2017.
- [8] Holund Elektronikk AS. DAB Magnetic base antenna, model 202-856. <http://www.holund.no/file/andre/datablad-202-856.pdf>. Accessed:13/06/2017.
- [9] TT Micro. Tiny audio - antenne ad01. <http://www.ttmicro.no/dab-i-bil/antenner/tiny-audio-antenne-ad01-erstatnant-for-c3-c5-c6-c10-og-c11-101477-p0000006606>. Accessed:13/06/2017.

## BIBLIOGRAPHY

---

- [10] 'leetghostdriver'. Opel Astra line-art, Deviantart.com. <http://leetghostdriver.deviantart.com/art/Opel-Astra-line-art-106672435>. Accessed:22/06/2017.
- [11] SCAN Antenna A/S. HE2M UNIVERSAL (FME) Flexible Helical whip antenna with FME-connector. <http://www.scan-antenna.com/product/he2m-universal-fme>. Accessed:13/06/2017.
- [12] DJI. Spreading wings s1000+ your dslr in flight. <https://www.dji.com/spreading-wings-s1000-plus>, . Accessed:12/06/2017.
- [13] Pablo Sánchez at Grab CAD Community. DJI S1000 CAD model. <https://grabcad.com/library/dji-s1000-1>. Accessed:11/02/2017.
- [14] Norwegian Communications Authority Nkom. Vurdering om dekningsvilkår for avvikling av FM er oppfylt, Dekningsvurderinger for NRKs DAB-nett, de kommersielle DAB-nettene og NRK P1s stereodekning i FM-nettet. [https://www.nkom.no/aktuelt/nyheter/\\_attachment/16724?\\_ts=14b963eaf69](https://www.nkom.no/aktuelt/nyheter/_attachment/16724?_ts=14b963eaf69), 2015. Accessed:13/06/2017.
- [15] International Telecommunication Union ITU. Final Acts of the Regional Radio-communication Conference for planning of the digital terrestrial broadcasting service in parts of Regions 1 and 3, in the frequency bands 174-230 MHz and 470-862 MHz (RRC-06). <http://handle.itu.int/11.1002/pub/801af205-en>, 2006. Accessed:13/06/2017.
- [16] United States Air Force. Mq-1b predator. <http://www.af.mil/About-Us/Fact-Sheets/Display/Article/104469/mq-1b-predator/>, September 2015. Accessed 07/06/17.
- [17] General Atomics. General atomics company. <http://www.ga.com/>, 2017. Accessed 07/06/17.
- [18] U.S.Air Force. United states air force. <https://www.airforce.com/>. Accessed:14/06/2017.
- [19] DJI. Dji company. <http://www.dji.com/company>, . Accessed 07/06/17.
- [20] H. Bendea, A. Cina, A. Lingua, P. Maschio, A. Olivieri, M. Piras, G. Virone. Measurements of the RF Antenna pattern using a Unmanned Aerial Vehicle (UAV): test and results. *Politecnico di Torino, First National Meeting on Science and Technology with SKA*, 2012.
- [21] Nkom. The Norwegian Communications Authority. <https://www.nkom.no/>. Accessed:26/11/2016.

- [22] Norwegian Government information website. Radio digitisation in 2017. <https://www.regjeringen.no/en/aktuelt/radio-digitisation-in-2017/id2406145/>. Accessed:14/06/2017.
- [23] European Telecommunications Standards Institute (ETSI). ETSI TS 102 563 V2.1.1 Digital Audio Broadcasting (DAB); DAB+ audio coding (MPEG HE-AACv2). ETSI, January 2017. [http://www.etsi.org/deliver/etsi\\_ts/102500\\_102599/102563/02.01.01\\_60/ts\\_102563v020101p.pdf](http://www.etsi.org/deliver/etsi_ts/102500_102599/102563/02.01.01_60/ts_102563v020101p.pdf). Accessed:18/06/2017.
- [24] PIXHAWK. Pixhawk PX4 autopilot. <https://pixhawk.org/>, 16/06/2017.
- [25] 3DR. 3DR uBlox GPS with Compass Kit. [https://3dr.com/support/articles/3dr\\_ublox\\_gps\\_with\\_compass\\_kit](https://3dr.com/support/articles/3dr_ublox_gps_with_compass_kit). Accessed:13/06/2017.
- [26] Signal Hound Inc. Signal Hound website. <https://signalhound.com>. Accessed:14/06/2017.
- [27] Odroid Wiki. <http://odroid.com/dokuwiki/doku.php?id=en:odroid-xu4>. Accessed: 2016-12-18.
- [28] Norwegian Communications Authority. Informasjon om Lokalradioblokka Oversikt over frekvensallokeringer og lokalregioner. *Nkom*, July 2012. [https://www.nkom.no/teknisk/frekvensauksjoner/auksjoner/planlagte-avsluttede/\\_attachment/4608?\\_ts=13b08f11bb5](https://www.nkom.no/teknisk/frekvensauksjoner/auksjoner/planlagte-avsluttede/_attachment/4608?_ts=13b08f11bb5). Accessed:10/02/2017.
- [29] Antenna-Theory.com. Antenna-Theory. <http://www.antenna-theory.com/>. Accessed:15/06/2017.
- [30] David M. Pozar. *Microwave and RF Design of Wireless Systems*. John Wiley & Sons, Inc, 2001. ISBN 0471322822.
- [31] Constantine A. Balanis. *Antenna theory : Analysis and Design*. John Wiley & Sons, Fourth edition, 2016. ISBN 9781118642061.
- [32] IEEE Standard Definitions of Terms for Antennas. *IEEE Std 145-1993*, pages 1–32, July 1993. doi: 10.1109/IEEESTD.1993.119664.
- [33] 'GlenDash' Glen Dash, Ampyx LLC. How RF Anechoic Chambers Work. [http://www.glendash.com/Dash\\_of EMC/Anechoic\\_Chambers/Anechoic\\_Chambers.pdf](http://www.glendash.com/Dash_of EMC/Anechoic_Chambers/Anechoic_Chambers.pdf), Copyright 1999, 2005 Ampyx LLC. Accessed:15/06/2017.
- [34] L. Meier, D. Honegger, and M. Pollefeys. PX4: A node-based multithreaded open source robotics framework for deeply embedded platforms. In *Robotics and Automation (ICRA), 2015 IEEE International Conference on*, may 2015.

## BIBLIOGRAPHY

---

- [35] u-blox. Neo-7 series u-blox 7 gnss modules. <https://www.u-blox.com/en/product/neo-7-series>. Accessed:13/06/2017.
- [36] Hardkernel. Hardkernel website. <http://www.hardkernel.com/main/main.php>. Accessed: 18/12/2016.
- [37] BEMA. Aktiv DAB/DAB+ antenne med vinkelplugg (AD01). <http://www.bema.no/?itemID=34413>. Accessed:16/06/2017.
- [38] Benton County Arkansas. Coaxial Cable Loss and Dynamics Page, RG-316 cable loss. <http://www.bcar.us/cablespec.htm>. Accessed:13/06/2017.
- [39] Dassault Systemes SolidWorks Corporation. SolidWorks 3D software tool. <http://www.solidworks.no>. Accessed:16/06/2017.
- [40] Efobasen Elektro foreningen. Castor EC16 electrical pvc pipe clip, El.nr.1323120. <http://efobasen.efo.no/produkt-detaljer?pn=1323120>. Accessed: 19/06/2017.
- [41] PoliTo. Politecnico di torino. <http://www.polito.it/>. Accessed:14/06/2017.

# Appendix A

## Mission list

CMD	TimeUS	CTot	CNum	CId	Prm1	Prm2	Prm3	Prm4	Lat	Lng	Alt
CMD	75467441	12	1	18	1	0	20	0	63.319080399999997	10.2735062	3
CMD	75467460	12	2	18	1	0	-20	0	63.319080399999997	10.2735062	3
CMD	75467480	12	3	18	1	0	19	0	63.319080399999997	10.2735062	6
CMD	75467499	12	4	18	1	0	18	0	63.319080399999997	10.2735062	10
CMD	75467519	12	5	18	1	0	17	0	63.319080399999997	10.2735062	13
CMD	75467538	12	6	18	1	0	15	0	63.319080399999997	10.2735062	16
CMD	75467601	12	7	18	1	0	13	0	63.319080399999997	10.2735062	18
CMD	75467620	12	8	18	1	0	10	0	63.319080399999997	10.2735062	20
CMD	75467639	12	9	18	1	0	7	0	63.319080399999997	10.2735062	22
CMD	75467687	12	10	18	1	0	3	0	63.319080399999997	10.2735062	23
CMD	75467706	12	11	17	0	0	1	0	63.319080399999997	10.2735062	23

Table A.1: Waypoint list for the GNSS positions used for the measurements.

APPENDIX A. MISSION LIST

---



## **Appendix B**

**Azimuth plane measurement data at  
elevation angle  $\theta = 28^\circ$**

## B.1 Magnetic base roof mounted antenna

The received power in dBm measured for the magnetic base antenna in the azimuth plane at elevation angle  $\theta = 28^\circ$ .

No	Received dBm	Azimuth angle $\phi$	No	Received dBm	Azimuth angle $\phi$
1	-60,4093	278,26	23	-63,4056	123,21
2	-61,9619	285,16	24	-65,3032	133,07
3	-62,2476	293,66	25	-65,4267	143,03
4	-61,4250	305,79	26	-64,6553	153,20
5	-60,3527	316,98	27	-64,6544	163,10
6	-59,7366	325,14	28	-64,6770	171,49
7	-59,4389	333,55	29	-64,3417	179,27
8	-59,6020	342,00	30	-64,3916	186,52
9	-59,8331	350,49	31	-64,3905	193,53
10	-60,2051	358,88	32	-64,3658	200,61
11	-61,0967	7,22	33	-65,5898	207,73
12	-62,8476	15,78	34	-67,8514	215,12
13	-63,0144	24,45	35	-67,6857	224,17
14	-62,5032	33,63	36	-65,6699	239,45
15	-61,8133	43,34	37	-65,4319	249,89
16	-61,8093	52,98	38	-64,1633	254,84
17	-61,7292	62,63	39	-62,9064	254,11
18	-61,3811	75,03	40	-63,1326	257,12
19	-61,3693	86,48	41	-63,4569	263,36
20	-61,8675	95,63	42	-62,7725	271,22
21	-62,1515	104,70	43	-62,2432	279,03
22	-61,9911	113,66	44	-60,4093	278,26

Table B.1: Measurements results for the magnetic base roof mounted antenna in the azimuth plane at elevation angle  $\theta = 28^\circ$ .

## B.2 Windshield mounted antenna

The received power in dBm measured for the windshield mounted antenna in the azimuth plane at elevation angle  $\theta = 28^\circ$ .

No	Received dBm	Azimuth angle $\phi$	No	Received dBm	Azimuth angle $\phi$
1	-94,9009	278,68	24	-91,2887	120,63
2	-93,1605	282,63	25	-93,7547	129,50
3	-91,6072	287,28	26	-92,8707	137,71
4	-90,3045	296,20	27	-94,9643	144,71
5	-89,0722	302,60	28	-94,8997	151,34
6	-88,1465	309,50	29	-93,8245	157,81
7	-88,4061	316,95	30	-91,9380	165,05
8	-90,8619	324,81	31	-92,0977	176,53
9	-91,3612	332,99	32	-92,4148	185,79
10	-87,0039	341,59	33	-92,0746	195,39
11	-84,3375	351,08	34	-92,5934	204,80
12	-84,4330	1,50	35	-94,3172	222,21
13	-87,3098	14,94	36	-94,1523	233,39
14	-93,2284	24,64	37	-95,6598	244,74
15	-94,7193	34,29	38	-94,7356	256,44
16	-90,5435	43,66	39	-94,7220	262,64
17	-88,5493	53,10	40	-95,7925	261,35
18	-89,5776	62,25	41	-95,8390	264,03
19	-91,3161	71,55	42	-96,8132	269,13
20	-90,5989	80,65	43	-95,1460	274,28
21	-88,1620	89,15	44	-100,726	280,21
22	-86,3488	97,46	45	-94,9009	278,68
23	-87,2177	105,37			

Table B.2: Measurements results for the windshield mounted antenna in the azimuth plane at elevation angle  $\theta = 28^\circ$ .